

# Insight into the outer membrane asymmetry of *P. aeruginosa* and the role of MlaA in modulating the lipidic composition, mechanical, biophysical, and functional membrane properties of the cell envelope

M. Kaur,<sup>1</sup> N. Mozaheb,<sup>1</sup> T. O. Paiva,<sup>2</sup> M.-F. Herent,<sup>3</sup> F. Goormaghtigh,<sup>1</sup> A. Paquot,<sup>4</sup> R. Terrasi,<sup>4</sup> E. Mignolet,<sup>5</sup> J.-L. Décout,<sup>6</sup> J. H. Lorent,<sup>1</sup> Y. Larondelle,<sup>5</sup> G. G. Muccioli,<sup>4</sup> J. Quetin-Leclercq,<sup>3</sup> Y. F. Dufrière,<sup>2</sup> M.-P. Mingeot-Leclercq<sup>1</sup>

**AUTHOR AFFILIATIONS** See affiliation list on p. 20.

**ABSTRACT** In Gram-negative bacteria, the outer membrane (OM) is asymmetric, with lipopolysaccharides (LPS) in the outer leaflet and glycerophospholipids (GPLs) in the inner leaflet. The asymmetry is maintained by the Mla system (MlaA-MlaBCDEF), which contributes to lipid homeostasis by removing mislocalized GPLs from the outer leaflet of the OM. Here, we ascribed how *Pseudomonas aeruginosa* ATCC 27853 coordinately regulates pathways to provide defense against the threats posed by the deletion of *mlaA*. Especially, we explored (i) the effects on membrane lipid composition including LPS, GPLs, and lysophospholipids, (ii) the biophysical properties of the OM such as stiffness and fluidity, and (iii) the impact of these changes on permeability, antibiotic susceptibility, and membrane vesicles (MVs) generation. Deletion of *mlaA* induced an increase in total GPLs and a decrease in LPS level while also triggering alterations in lipid A structures (arabinylation and palmitoylation), likely to be induced by a two-component system (PhoPQ-PmrAB). Altered lipid composition may serve a physiological purpose in regulating the mechanobiological and functional properties of *P. aeruginosa*. We demonstrated an increase in cell stiffness without alteration of turgor pressure and inner membrane (IM) fluidity in  $\Delta mlaA$ . In addition, membrane vesiculation increased without any change in OM/IM permeability. An amphiphilic aminoglycoside derivative (3',6'-dinonyl neamine) that targets *P. aeruginosa* membranes induced an opposite effect on  $\Delta mlaA$  strain with a trend toward a return to the situation observed for the WT strain. Efforts dedicated to understanding the crosstalk between the OM lipid composition, and the mechanical behavior of bacterial envelope, is one needed step for designing new targets or new drugs to fight *P. aeruginosa* infections.

**IMPORTANCE** *Pseudomonas aeruginosa* is a Gram-negative bacterium responsible for severe hospital-acquired infections. The outer membrane (OM) of Gram-negative bacteria acts as an effective barrier against toxic compounds, and therefore, compromising this structure could increase sensitivity to antibiotics. The OM is asymmetric with the highly packed lipopolysaccharide monolayer at the outer leaflet and glycerophospholipids at the inner leaflet. OM asymmetry is maintained by the Mla pathway resulting in the retrograde transport of glycerophospholipids from the OM to the inner membrane. In this study, we show that deleting *mlaA*, the membrane component of Mla system located at the OM, affects the mechanical and functional properties of *P. aeruginosa* cell envelope. Our results provide insights into the role of MlaA, involved in the Mla transport pathway in *P. aeruginosa*.

**Editor** Eric Cascales, Centre National de la Recherche Scientifique, Marseille, France

Address correspondence to M.-P. Mingeot-Leclercq, marie-paule.mingeot@uclouvain.be.

N. Mozaheb and T. O. Paiva contributed equally to this article.

The authors declare no conflict of interest.

See the funding table on p. 20.

**Received** 10 July 2024

**Accepted** 14 August 2024

**Published** 7 October 2024

Copyright © 2024 Kaur et al. This is an open-access article distributed under the terms of the [Creative Commons Attribution 4.0 International license](https://creativecommons.org/licenses/by/4.0/).

**KEYWORDS** *P. aeruginosa*, outer membrane, membrane biophysics, lipids, cell envelope

In Gram-negative bacteria, like *Pseudomonas aeruginosa*, the cell envelope is made up of an inner phospholipid bilayer (IM), a periplasm that contains a thin peptidoglycan cell wall and an outer membrane (OM) presenting an asymmetric distribution of lipids on both leaflets. The outer leaflet is almost exclusively composed of lipopolysaccharides (LPS), whereas the inner leaflet mainly contains glycerophospholipids (GPLs). LPS is a negatively-charged amphiphilic molecule composed of three covalently linked moieties: lipid A, a core oligosaccharide, and a polysaccharide called O-antigen. GPLs are mainly phosphatidylethanolamine (PE), phosphatidylglycerol (PG), and cardiolipin (CL), which are also found in the inner membrane (1).

The asymmetric distribution of LPS and GPLs in the OM is critical for maintaining membrane mechanical properties required for cell fitness and protection against environmental stress and antibiotics. This is elucidated by the fact that a loss of OM asymmetry is responsible for a decrease in permeability barrier function (2, 3), a reduction in virulence (4–7), and the dwindling of intrinsic resistance to some antimicrobials (8–10).

The maintenance of lipid asymmetry is therefore crucial and is in part controlled by the Mla (MlaA/VacJ-MlaC-MlaFEDB) system. The Mla system, composed of 6 proteins, facilitates retrograde phospholipid transport from the OM back to the IM (11). The MlaA (also annotated as VacJ) component is highly conserved among Gram-negative bacteria (Table 1). It was first identified in *Shigella flexneri* as virulence-associated protein chromosome locus J (6). It is an integral alpha-helical OM protein (12) that transfers phospholipids from the outer leaflet of OM to the soluble periplasmic MlaC with no preference for specific phospholipids (13). MlaC (14) transfers the phospholipids to the multicomponent system MlaFEDB (13, 15). This ATP-binding-cassette (ABC) transport system in the IM comprises the IM permease MlaE, the IM ABC-type ATPase MlaF, the periplasmic subunit of MlaFEDB MlaD, which is anchored in the IM by a transmembrane helix, and a cytoplasmic accessory protein MlaB (13, 16).

In addition to the Mla system, lipid asymmetry in Gram-negative bacteria is maintained by the OM-phospholipase PldA (17, 18) and the palmitoyl transferase PagP (19). PldA cleaves GPLs at the *sn*-1 or *sn*-2 position, generating fatty acids and lysophospholipids (20), which can flip to the inner leaflet of the OM, where they are trafficked back to the IM by poorly understood mechanisms. Phospholipids at the inner leaflet of the OM are typically inaccessible to the active site of PldA (17, 21, 22). Disturbance of the OM integrity and asymmetry leads to the activation of PldA via a Ca<sup>2+</sup>-dependent dimerization mechanism (22, 23). PagP regulates lipid asymmetry of the OM by transferring *sn*-1 palmitate (C:16) from GPLs at the inner leaflet to lipid A at the outer leaflet, producing palmitoylated lipid A (11). Palmitoylated lipid A increases membrane

**TABLE 1** MlaA amino acids sequence conservation in *P. aeruginosa* and other Gram-negative bacteria

Microorganisms	Accession number	MlaA/VacJ	Amino acids
<i>P. aeruginosa</i>	AVK06939.1	100%	234
<i>Pseudomonas putida</i>	AFO47095.1	69.36%	235
<i>Pseudomonas syringae</i>	QWB08392.1	66.67%	233
<i>Acinetobacter baumannii</i>	BCR39766.1	41.75%	299
<i>Neisseria gonorrhoeae</i>	WP_010951410.1	38.39%	277
<i>Campylobacter jejuni</i>	EDP6655880.1	36.65%	232
<i>Caulobacter crescentus</i>	QXZ52028.1	36.70%	286
<i>Vibrio cholerae</i>	ACP06275.1	35.84%	254
<i>Haemophilus influenzae</i>	AIT66950.1	33.82%	250
<i>Shigella flexneri</i> 2 a	NP_708228.1	33.04%	251
<i>Escherichia coli</i>	QKU50363.1	33.04%	251
<i>Salmonella enterica typhimurium</i>	WP_000776787.1	32.17%	251

hydrophobicity (24) and activates the periplasmic  $\sigma^E$  stress response (25). PagP activity is an established marker for monitoring ectopic GPL exposure in the OM of *E. coli* (26, 27) and accumulation of GPLs in the outer leaflet of the OM in cells lacking MlaA (4, 11). On *Klebsiella pneumoniae* (24) and *Salmonella typhimurium* (28), PagP showed a bifunctional activity with additional capacity to transfer a palmitoyl moiety to PG, which also increases membrane hydrophobicity (24) and promotes the generation of membrane vesicles (MVs) (28).

Regulating cell wall properties, including lipid asymmetry, plays a key role in antibiotic resistance and bacterial survival and thus might provide a source for antibiotic targets. Since the OM is the first place where antibiotics interact with the bacteria, we selected to focus on the protein from the Mla system, located at the OM, MlaA. On *P. aeruginosa* WT and  $\Delta mlaA$ , we characterized the lipidic composition, the mechanical and biophysical properties of the cell envelope, and the significance of changes induced by *mlaA* deletion. Especially, we explored the effects of *mlaA* deletion on (i) the lipid composition of membranes including LPS, GPLs, and lysophospholipids, (ii) the biophysical properties of the OM (stiffness, fluidity, etc.), and (iii) the impact of these changes on permeability, antibiotic susceptibility, and MVs generation. All studies were conducted in the presence and absence of the amphiphilic aminoglycoside derivative, 3',6'-dinonyl neamine (3',6'-diNn), known to bind to the main components of the OM, LPS (29), and GPLs (30, 31).

## RESULTS

### Characterization of *P. aeruginosa* $\Delta mlaA$ strain

Gene-specific PCR followed by electrophoresis was performed on DNA extracted from *P. aeruginosa* WT and  $\Delta mlaA$ . We confirmed the deletion of *mlaA* (Fig. S1C). The mRNA expression of other *mla* genes (*mlaB*, *mlaC*, *mlaD*, *mlaE*, and *mlaF*) in  $\Delta mlaA$  over WT strain showed an increase from 1.3-fold to 2.6-fold (Fig. S1D). *P. aeruginosa* strains, WT,  $\Delta mlaA$ , and  $\Delta mla att7::m laA$  did not show any differences in growth curves, intracellular survival, and morphology (5).

### Deletion of *m laA* induced an increase in glycerophospholipids (GPLs) at the OM of *P. aeruginosa*. 3',6'-dinonyl neamine increased GPLs in the WT strain but not in *P. aeruginosa* $\Delta m laA$

The Mla system maintains OM-lipid asymmetry and traffics GPLs between the OM and IM bilayers (11, 32, 33). We hypothesized that *m laA* deletion induced altered OM lipid composition. Therefore, we determined the total amounts of GPLs in the OM of *P. aeruginosa* WT and  $\Delta m laA$ . We then investigated the changes in individual GPLs, including phosphatidylethanolamine (PE), phosphatidylglycerol (PG), and cardiolipin (CL). To assess the potential role of PldA and/or PagP, we monitored the amounts of lyso-derivatives (lysophosphatidylethanolamine, LPE; lysophosphatidylglycerol, LPG). The degree of unsaturation was determined as well.

Focusing on total GPLs, we showed that deletion of *m laA* ( $\Delta m laA$ ) increased total GPLs in *P. aeruginosa* OM (110%  $\pm$  6%) in comparison with *P. aeruginosa* WT (Fig. 1A). A deeper analysis of individual lipid headgroups (PE, PG, and CL) (Fig. 1B) revealed a significant increase in PE in  $\Delta m laA$  strain compared with WT bacteria (Fig. S3A). The increase was significant for the PE species (16:0\_16:1, 16:0\_16:2, 16:0\_18:1, and 18:1\_18:2) (Fig. S2A).

The addition of 3',6'-dinonyl neamine on *P. aeruginosa* WT induced a significant increase in GPLs (117%  $\pm$  7%), whereas no significant change was observed when adding the compound to *P. aeruginosa*  $\Delta m laA$  (Fig. 1A). In WT strain, an analysis on the individual GPL species showed a significant increase in one CL species (72:0) (Fig. S2C) without any significant global change for PE, PG, and CL (Fig. S3A). In *P. aeruginosa*  $\Delta m laA$ , incubation with 3',6'-dinonyl neamine did not alter the glycerophospholipids species (Fig. S2A through C and S3A).

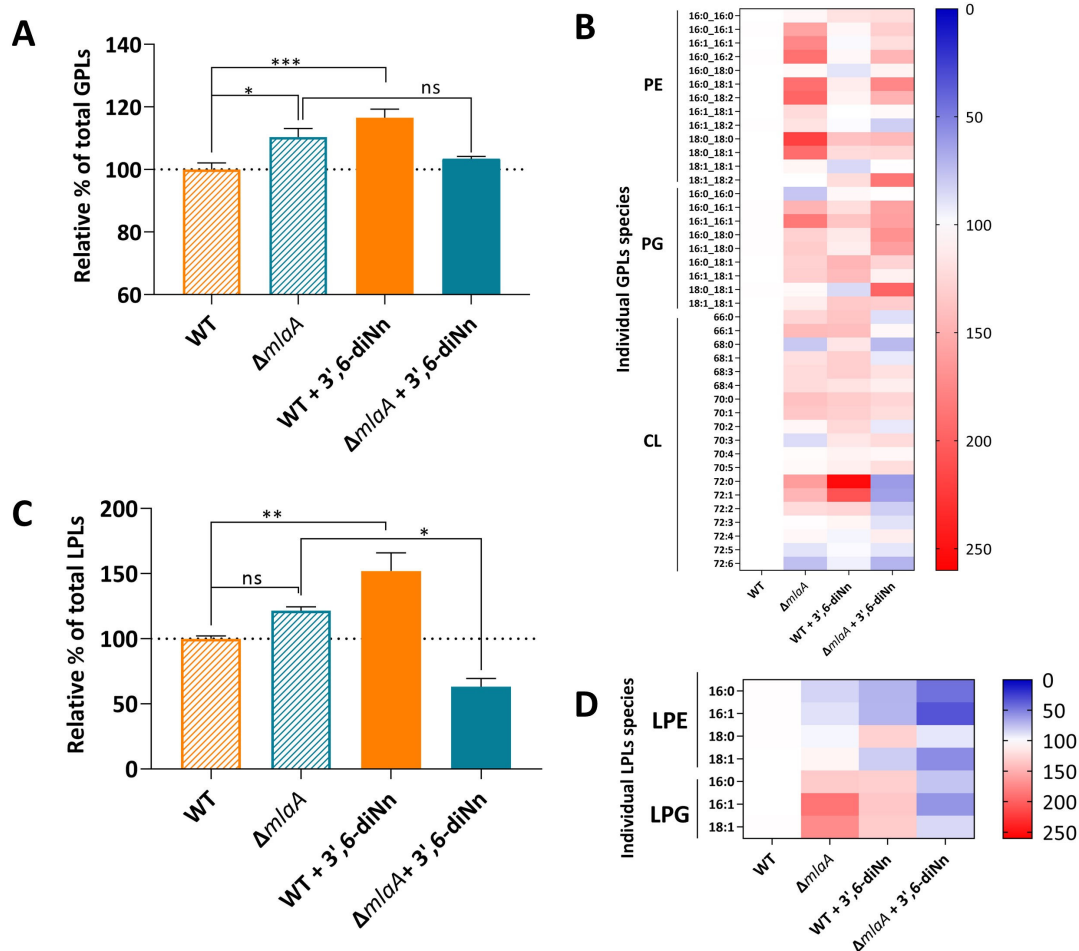


**FIG 1** Glycerophospholipids and lysophospholipids profile *P. aeruginosa* WT and  $\Delta mlaA$  in the presence or absence of 3',6-dinonyl neamine (1 $\times$  MIC, 2  $\mu$ g/mL, 1 h). (A and C) Total glycerophospholipids. (B and D) Heat maps of individual glycerophospholipids and lysophosphoglycerides species. Red-filled, blue-filled, and white-filled lines referred to increased, decreased, and unchanged levels of lipid structures, respectively. Total lipids were determined by using a fluorescent probe FM4-64, and individual lipids PE, PG, CL, LPE, and LPG were analyzed by LC-MS. The results are expressed in % where WT is considered 100%. Statistical analysis was performed using one-way ANOVA with Tukey's multiple-comparison test. (A and C) \*\*\* $P$  < 0.001, \*\* $P$  < 0.01, \* $P$  < 0.05; <sup>ns</sup>  $P$  > 0.05.

The presence of higher amounts of GPLs at the OM of *P. aeruginosa*  $\Delta mlaA$  might activate enzymes like PldA and/or PagP, resulting in the production of lyso-derivatives (34). Lysophospholipids are the products of GPLs hydrolysis by endogenous PldA or by-products of PagP. Interestingly, the profile of total lyso-derivatives was similar to that observed for GPLs with a tendency that lyso-derivatives in OM of *P. aeruginosa*  $\Delta mlaA$  strain increased (122%  $\pm$  4%) when compared with WT (100%  $\pm$  4%) (Fig. 1C). At the headgroup level (Fig. 1D), the increase mostly resulted from LPE compared with LPG (Fig. S2D and S3B). As for GPLs, the addition of 3',6-dinonyl neamine resulted in an increase in total lyso-derivatives in WT (152%  $\pm$  20%) (Fig. 1C) resulting from the increase in LPG (Fig. S3B). In *P. aeruginosa*  $\Delta mlaA$ , a huge decrease (66%  $\pm$  8%) in lyso-derivatives was observed upon the addition of the compound (Fig. 1C), which affected both LPE and LPG (Fig. S3B).

Comparing lipid acyl chains, we observed that monounsaturated and polyunsaturated acyl chains increased in *P. aeruginosa*  $\Delta mlaA$  compared with WT (Fig. 1B; Fig. S3C). Addition of 3',6-dinonyl neamine on *P. aeruginosa* WT increased the three subtypes of acylated chains with a significant effect observed for saturated chains (Fig. 1B and D; Fig. S2A through D and S3C), whereas no significant change was observed for  $\Delta mlaA$  strain (Fig. 1B; Fig. S2A through D and S3C).

In conclusion, the deletion of *mlaA* induced an increase in the amounts of GPLs at the OM of *P. aeruginosa* with a major effect on PE. 3',6'-dinonyl neamine increased GPLs in the WT strain without any significant changes in *P. aeruginosa*  $\Delta mlaA$ .

### Deletion of *mlaA* in *P. aeruginosa* induced a decrease in LPS and a increase in lipid A modifications by increasing palmitoylation and arabinosylation. Higher expression of two two-component systems, PhoPQ and PmrAB, is observed as well

Perturbing OM asymmetry results in signal transduction across the periplasm and a lipid-mediated regulatory mechanism that controls LPS biosynthesis (17, 35). Accordingly, we hypothesized that *mlaA* deletion might influence the LPS levels in *P. aeruginosa*. Relative to the WT strain, the LPS levels of the  $\Delta mlaA$  strain were significantly decreased (by 75%) (Fig. 2), similar to what was reported for  $\Delta mlaF$  mutant of *A. baumannii* (36). The effect of 3',6'-dinonyl neamine is dependent upon the presence of MlaA, with a decrease in WT (by 19%) and a huge increase in  $\Delta mlaA$  (Fig. 2A) strain (293%).

To know whether the decrease in LPS content in *P. aeruginosa*  $\Delta mlaA$  is accompanied by structural modifications of the LPS moiety embedded in lipids (lipid A), we explored the activation of two two-component systems (TCSs), PhoP-PhoQ and PmrA-PmrB (37). In these systems, a sensory kinase, that is, PhoQ or PmrB, is located at the IM and is activated by an environmental signal, which in turn phosphorylates a cytoplasmic transcriptional regulator, PhoP or PmrA, respectively. PhoPQ and PmrAB are involved in OM remodeling by lipid A modifications in LPS through palmitoylation via PagP, which transfers a palmitoyl group from a GPL to the  $\beta$ -OH of the 3'-O-acyl fatty acyl group, deacylation via PagL, which removes 3-OH C:10, arabinosylation via ArnT, which adds 4-amino-4-deoxy-L-arabinose to one or both of the 1 and 4'-phosphate groups, and/or hydroxylation of secondary acyl chains via LpxO1 and LpxO2.

Deletion of *mlaA* ( $\Delta mlaA$ ) led to the increased expression of the *pmrB* (2.1-fold), as well as the TCSs-induced lipid A modification genes (*pagP* 2.7-fold and *arnT* 2.2-fold) without any effect on *pmrA*, *phoP*, *phoQ*, and *pagL* (Fig. 2B). Upregulation of *pagP*, and *arnT* also reported in *Salmonella enterica* subsp. *enterica* serovar *Typhimurium*, helps to stabilize the OM, with an ultimate decrease in membrane fluidity and an increase in the surface charge (38, 39). Exposure of *P. aeruginosa* WT to 3',6'-dinonyl neamine induced an increase in the expression of *pmrB* (2.1-fold), *phoQ* (1.7-fold), and *arnT* (2.2-fold) (Fig. 2B). In the  $\Delta mlaA$  strain, 3',6'-dinonyl neamine exposure decreased the expression of *pagP* (by 33%) (Fig. 2B).

To further assess changes in lipid A, we used high-resolution mass spectrometry. Overall, the mass spectrum of lipid A characterized 14 single-charged [M-H]<sup>-</sup> and seven double-charged [M-2H]<sup>2-</sup> lipid A structures that were tri-, tetra-, penta-, or hexa-acylated. Among these, some were palmitoylated and/or arabinosylated (Fig. 2C and D; Tables S2 and S3). In *P. aeruginosa* WT and  $\Delta mlaA$ , before as well as after the treatment with 3',6'-dinonyl neamine, the most intense ion was *m/z* of 1365.89 (PLA1), which represents a mono-phosphate penta-acylated lipid A form (see detailed results in the supplementary part). Furthermore, we determined the levels of lipid A acyl chains after normalization to total LPS via derivatization/gas chromatography (Fatty Acid Methyl Esters; FAMES) (Fig. 2A). We observed an increase in 2-OH C12:0, 3-OH C12:0 in *P. aeruginosa*  $\Delta mlaA$  compared with WT strain. How these changes are related to the activity of LpxO1/2 known to  $\alpha$ -hydroxylate the 2'- and 2- secondary acyl chains of lipid A (40) is unclear. C16:0 also increased in the *P. aeruginosa*  $\Delta mlaA$  but decreased upon treatment with 3',6'-dinonyl neamine (Fig. 2E), consistent with the expression of *pagP* (Fig. 2B).

In summary, the absence of *mlaA* induced lipid A modifications through potential activation of PhoPQ and PmrAB TCSs, which in turn induced lipid A palmitoylation and arabinosylation. 3',6'-dinonyl neamine also induced lipid A modifications through activation of PhoPQ and PmrAB, increasing mRNA expression of *pagP*, *pagL*, and *arnT* in *P. aeruginosa* WT, whereas a decrease in mRNA expression of *pagP* was observed in  $\Delta mlaA$  strain. The increase of arabinosylation is in line with the increase in zeta potential

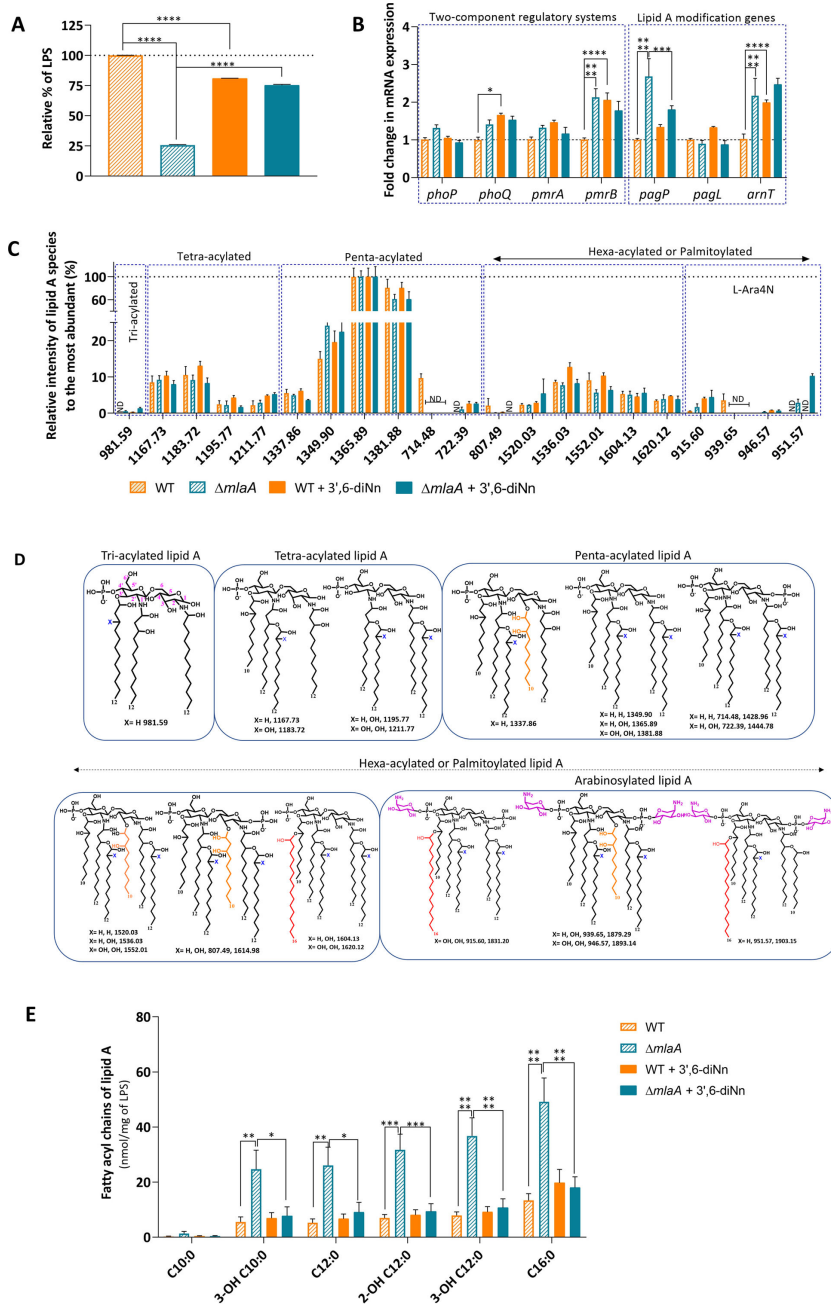


**FIG 2** Lipopolysaccharides (LPS) and lipid A modifications in *P. aeruginosa* WT and  $\Delta mlaA$  non-treated and treated with 3',6-dinonyl neamine (1 $\times$  MIC, 2  $\mu$ g/mL, 1 h). (A) Total LPS was measured by purpald assay. The results are expressed in relative % over *P. aeruginosa* WT, considered 100% (13,444  $\pm$  16  $\mu$ g/mL). (B) mRNA expression of two-component regulatory systems (*phoP*, *phoQ*, *pmrA*, and *pmrB*) and lipid A modifications genes (*pagP*, *pagL*, and *arnT*). The results are expressed in fold change over *P. aeruginosa* WT. (C) MS peaks (*m/z*) obtained by ESI-MS (negative ion mode) shown in different boxes as tri-acylated, tetra-acylated, penta-acylated, hexa-acylated, palmitoylated, and arabinosylated with their relative intensity compared with the major peak for each condition (*m/z* 1365.89). (D) Predicted structures of lipid A structures from *m/z* were obtained. The positions of the acyl chain are hypothetical; 4-aminoarabinose added by ArnT is shown in purple, and palmitate chain added by PagP is shown in red on lipid A structures. (E) Fatty acids were isolated from lipid A structures and analyzed as FAMES using gas chromatography - mass spectrometry (GC-MS). Statistical analysis was performed by two-way ANOVA with multiple comparisons (B, C, E) and one-way ANOVA with Tukey's multiple-comparison test (A) \*\*\*\**P* < 0.0001, \*\*\**P* < 0.001, \**P* < 0.05, ND undetectable. All values are given in mean  $\pm$  SEM, and the experiment was repeated thrice.

(−31.8 mV in  $\Delta mlaA$  strain) compared with the WT strain (−37.6 mV) (Fig. S5). If and how these changes in OM lipid composition affect the mechanobiological properties of OM was the next question we addressed by using atomic force microscopy (AFM).

### Deletion of *mlaA* induced an increase in the stiffness of the cell envelope without altering the turgor pressure. 3',6-dinonyl neamine induced a higher softening of the cell envelope of the *P. aeruginosa* $\Delta mlaA$

AFM has emerged as a valuable multifunctional technique to investigate the structure and mechanical properties of microbial cells. In mechanobiology, AFM-based indentation experiments have enabled to quantify the mechanical properties of whole bacterial cells and isolated cell walls (41). Spatially resolved force-distance curves were collected on top of the bacteria (Fig. 3A), and respective elasticity (Fig. 3B) and stiffness (Fig. 3C) information was extracted from them (41, 42). Representative force-indentation curves are shown in Fig. 3A, for both *P. aeruginosa* WT and  $\Delta mlaA$  strains before and after treatment with 3',6-dinonyl neamine at the minimum inhibitory concentration (MIC) for 1 h. As expected for Gram-negative bacteria, the curves featured two regions, that is, a nonlinear regime at low forces reflecting cell wall elasticity, followed by a linear regime at high forces associated with turgor pressure. From these two regions, we calculated the bacterial Young's modulus,  $E$ , and the bacterial spring constant,  $k$  (43, 44). Representative distributions of  $E$  and  $k$  values are shown in Fig. 3B and C, respectively.

A Young's modulus of  $0.50 \pm 0.18$  MPa (mean  $\pm$  SD,  $n = 11$  cells) was measured for *P. aeruginosa* WT (Fig. 3D), a value higher than that of  $0.24$  MPa  $\pm$  0.04 published by Formosa et al (45), a difference that we attribute to intercellular variability and differences in experimental conditions.

Interestingly, the Young's modulus value here calculated for *P. aeruginosa* WT was slightly lower than those published for *E. coli* (ranging from 1 to a few MPa) (46–48). This difference can be explained by (i) the thinner peptidoglycan layer of *P. aeruginosa* compared with *E. coli* (49), (ii) a reduced interaction between peptidoglycan and the OM (50) and, (iii) differences in lipid composition as lower amounts of very long chain fatty acids covalently bonded to hopanoids (51) or the shorter fatty acyl chains of lipid A (C12) from *P. aeruginosa* compared with other Gram-negative bacteria including *A. baumannii* (C12–C14) and *Burkholderia mallei* (C14–C16) (52). Deletion of *mlaA* significantly increased Young's modulus (Fig. 3D) as it reached  $0.84 \pm 0.34$  MPa ( $n = 16$  cells), indicating a stiffening of the cell envelope.

A decrease in Young's modulus (Fig. 3D) to  $0.29 \pm 0.164$  MPa ( $n = 10$  cells) and  $0.22 \pm 0.10$  MPa ( $n = 12$  cells) was observed upon incubation with 3',6-dinonyl neamine, for the WT and  $\Delta mlaA$  strains, respectively.

The  $k$  values (Fig. 3E) were found to be similar for WT and *mlaA* deleted strains ( $0.015 \pm 0.003$  and  $0.015 \pm 0.004$  N/m,  $n = 11, 16$  cells), indicating similar levels of turgor pressure. These values are in the range of those reported by Yao et al for *P. aeruginosa* (0.02 N/m) (49) as well as for *Shewanella putrefaciens* (0.02–0.05 N/m), another Gram-negative bacterium (53). The spring constants here calculated for *P. aeruginosa* were lower compared with *E. coli* (0.04 N/m) (54, 55). Treatment with 3',6-dinonyl neamine resulted in a decrease of  $k$  to  $0.010 \pm 0.003$  N/m (WT,  $n = 10$  cells) and  $0.008 \pm 0.003$  N/m ( $\Delta mlaA$ ,  $n = 12$  cells), indicating a turgor pressure decrease as a result of the antibiotic action.

In parallel, AFM topographical characterization of the cell morphology was performed in quantitative imaging mode (Fig. 4). As can be seen in Fig. 4A, both WT and  $\Delta mlaA$  strains showed the characteristic rod shape of *P. aeruginosa* cells. No morphological differences were observed between the two strains, as confirmed by the high-resolution images recorded on top of the cells (Fig. 4B). Similar morphological features were observed upon treatment with 3',6-dinonyl neamine, with no significant changes detected on the surface ultrastructure as evaluated by AFM. Identical height values, extracted from the AFM images, were observed for *P. aeruginosa* cells from both before and after antibiotic treatment (Fig. S5). Importantly, this observation validates the use of

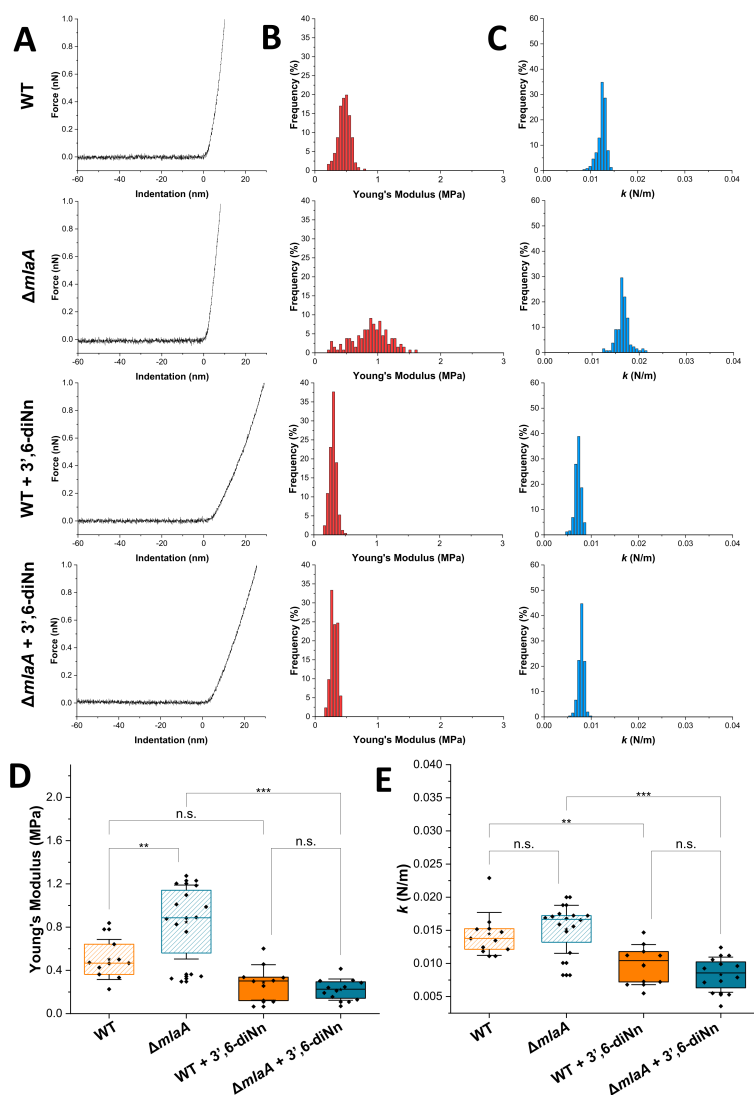


**FIG 3** Characterization of the cell envelope mechanics by AFM. (A) Representative force-indentation curves and distributions of (B) Young's modulus and (C) spring constant of one representative *P. aeruginosa* cell of WT and  $\Delta mlaA$  strains, before and after treatment with 3',6-dinonyl neamine (1 $\times$  MIC, 2  $\mu$ g/L, 1 h). (D) Box plot shows the Young's modulus, and (E) spring constant values were calculated from the force-indentation curves for both strains, before and after antibiotic treatment. (D and E) Statistical analyses were carried out using a statistical Tukey's multiple-comparison test. Stars indicate the mean values, lines the medians, boxes indicate the 25%–75% quartiles, and whiskers indicate the standard deviation obtained from at least 10 independent cells over at least three independent experiments \*\*\* $P \leq 0.001$ , \*\* $P \leq 0.01$ , and <sup>n.s.</sup>  $P > 0.01$ , determined by Tukey's multiple-comparison test.

AFM in the present study, excluding the role of possible AFM artifacts/interferences to the conclusions described above.

### Deletion of *mlaA* did not change IM fluidity in *P. aeruginosa*. 3',6-dinonyl neamine increased fluidity of IM in WT without any effect on $\Delta mlaA$ strain

Since the mechanical parameters of the cell envelope were changed, we were wondering if alterations of membrane biophysical parameters such as IM fluidity would also be affected. By using fluorescence-lifetime imaging microscopy (FLIM), we monitored the fluorescence lifetime of BODIPY-C10, which correlates with the viscosity of the environment in which the probe is embedded (56). In our analysis, a longer fluorescence lifetime



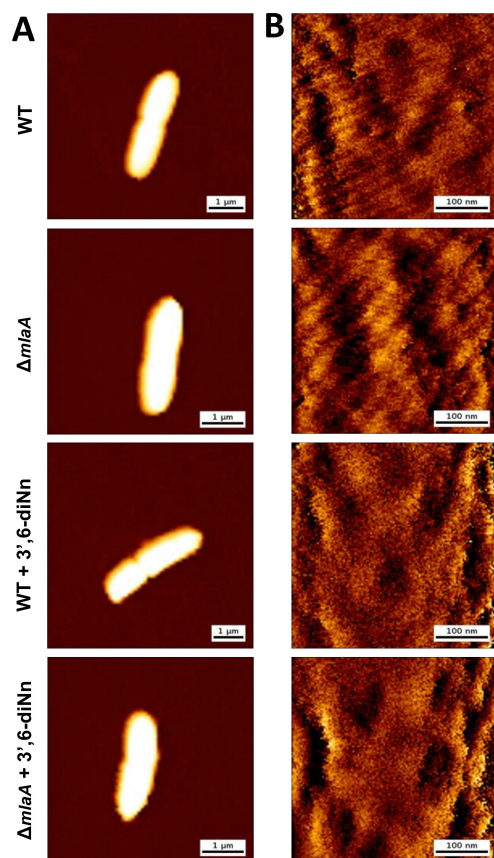


**FIG 4** AFM topographical characterization of *P. aeruginosa* WT and  $\Delta mIaA$  non-treated and treated with 3',6-dinonyl neamine ( $1\times$  MIC, 2 mg/L, 1 h). (A) Representative AFM height images of *P. aeruginosa* WT and  $\Delta mIaA$  strains, before and after treatment with antibiotic 3',6-dinonyl neamine ( $1\times$  MIC, 2  $\mu$ g/mL, 1 h). Color scale: 650 nm. (B) High-resolution height images were recorded on top of the cells. Color scale: 20 nm. The images were recorded in phosphate-buffered saline (PBS), and the cells were immobilized on glass-bottom dishes previously functionalized with poly-L-lysine.

of the probe indicates a higher viscosity or a lower fluidity of the membrane (57). The FLIM analysis showed that membrane fluidity of  $\Delta mIaA$  is similar to that of WT (Fig. 5A and B). 3',6-dinonyl increased fluidity in *P. aeruginosa* WT without any significant effect on *P. aeruginosa*  $\Delta mIaA$  (Fig. 5B).

#### **Deletion of *mIaA* did not change OM and IM permeability. *P. aeruginosa* $\Delta mIaA$ was less sensitive to OM permeabilization induced by 3',6 dinonyl neamine compared with WT, whereas no difference was observed in IM**

The amphipathic nature of LPS contributes to the permeability barrier of the OM (3). Changes in LPS contents and structural variations in lipid A may increase or decrease the permeation of hydrophobic compounds (58). We first determined OM and IM permeability in *P. aeruginosa* WT and  $\Delta mIaA$ . On both strains, we also evaluated the effect of 3',6-dinonyl neamine known to interact with LPS in the OM of *P. aeruginosa* (29). The OM permeability (Fig. 6A) was determined by using nitrocefin, a chromogenic  $\beta$ -lactam compound that undergoes a color change from yellow to red upon hydrolysis. In whole-cell Gram-negative bacteria,  $\beta$ -lactamases are primarily located in the periplasm; therefore, the nitrocefin hydrolysis rate is primarily limited by its diffusion rate across the OM (59). In the absence of antibiotics, both strains did not show any difference in OM permeability (10), suggesting no impact of *mIaA* deletion on OM permeability. Upon exposure to increasing concentrations of 3',6-dinonyl neamine (0–10  $\mu$ M), an increase in

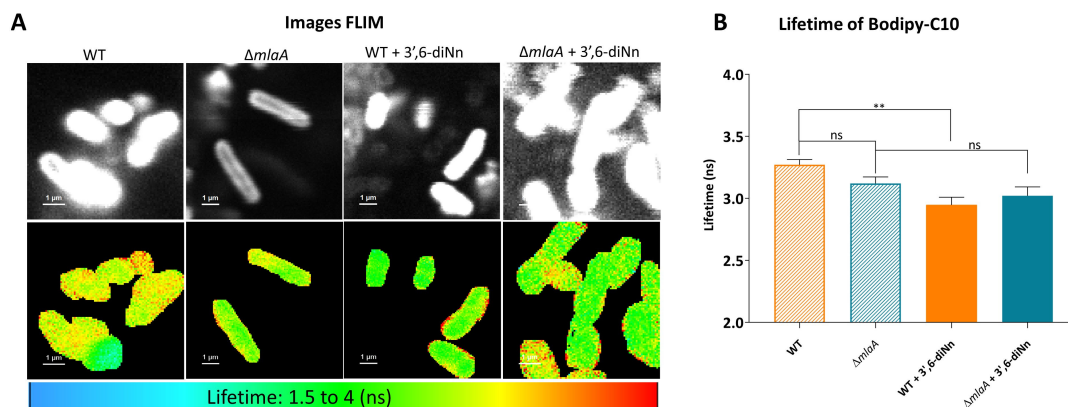


**FIG 5** FLIM images with their lifetime. *P. aeruginosa* WT and  $\Delta mlaA$  in the presence and absence of 3',6-dinonyl neamine (1× MIC, 2 mg/L, 1 h). (A) Top panels are intensity images, and the below panels are pseudo-colored FLIM images. (B) Lifetime measurements of the bacteria stained with BODIPY-C10. The data were obtained from two individual experiments, and in each experiment, at least 10 bacteria or three slides were considered to measure the lifetimes. The data are presented as means ± SD from three independent replicates. Statistical analysis was performed by one-way ANOVA with Tukey's multiple-comparison test. \*\* $P < 0.01$  and <sup>ns</sup>  $P > 0.05$ .

OM permeability was seen for both strains with a significant effect observed at 6 μM. At 8 μM and 10 μM, the effect was significantly higher for WT compared with  $\Delta mlaA$  strain (26% and 22%, respectively) (Fig. 6A). The decrease in LPS and the larger Young's modulus we observed for *P. aeruginosa*  $\Delta mlaA$  could explain the lower susceptibility of the OM to be permeabilized by 3',6-dinonyl neamine.

The IM permeability (Fig. 6B) was studied by propidium iodide, which fluoresces when it binds DNA. In the absence of an exogenous compound, no difference was observed for WT and *P. aeruginosa*  $\Delta mlaA$ . 3',6-dinonyl neamine induced a dose-dependent (0–10 μM) increase in IM permeability in both strains. At 6 μM and 8 μM, a significant effect was observed for  $\Delta mlaA$  and WT strains, respectively. In contrast with data for OM, no difference in IM permeabilization was observed between WT and  $\Delta mlaA$ , although the effect seemed slightly higher for *P. aeruginosa*  $\Delta mlaA$  (Fig. 6B).

### Deletion of *mlaA* induced a decrease (2-fold to 8-fold) in MIC of fluoroquinolones

To tentatively link membrane permeability to the antimicrobial activity of antibiotics, we determined the MICs in *P. aeruginosa* WT and  $\Delta mlaA$  for several antibiotics (abbreviations defined in Table 2). These included glycopeptides (VAN), lipoglycopeptides

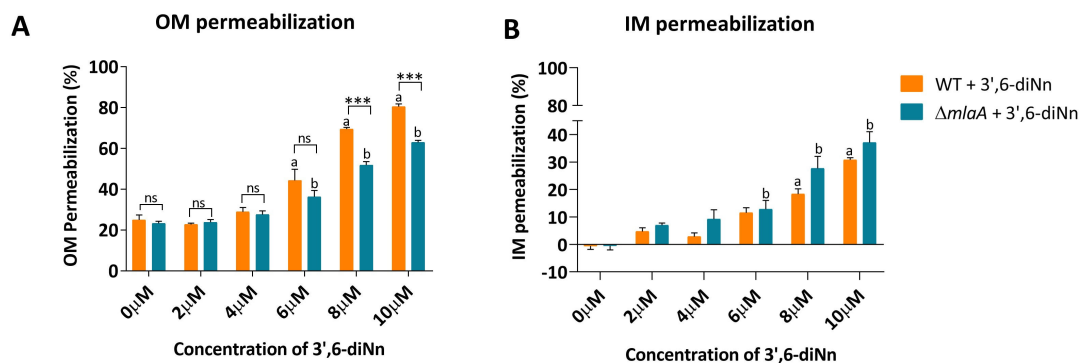


**FIG 6** Membrane permeabilization. (A) Outer membrane permeabilization was assessed by nitrocefin assay (B). Inner membrane permeabilization was assessed by propidium iodide assay where WT (orange) and  $\Delta mlaA$  (blue) were incubated with different concentrations (0–10 μM) of 3',6-dinonyl neamine. Statistical analysis was performed using two-way ANOVA with multiple comparisons. \*\*\* $P < 0.001$ ; <sup>ns</sup>  $P > 0.05$ ; (A and B) significant increase in membrane permeabilization compared with untreated *P. aeruginosa* WT (A) and  $\Delta mlaA$  (B).

**TABLE 2** Antibiotic susceptibility: MIC of different antibiotics determined for *P. aeruginosa* WT and  $\Delta mlaA$  ( $N = 3$ ), ND not determined

	Antibiotics	Generic abbreviation	Target/Process	MICs ( $\mu\text{g/mL}$ )	
				Wild-type	$\Delta mlaA$
Aminoglycosides	Amikacin	AMK	Binding to the aminoacyl site of 16S ribosomal RNA within the 30S ribosomal subunit	8	8
	Gentamicin	GEN		4	4
	Tobramycin	TOB		1	2
	Neomycin	NEO		128	>128
	Neamine	NEA		>512	>512
Amphiphilic aminoglycoside derivative	3',6-dinonyl neamine	3',6-diNn	Binding to the LPS & GPL domains	4	4
Polymyxin	Colistin	COL	Binding to the LPS	4	2
Fluoroquinolones	Ciprofloxacin	CIP	Inhibiting DNA gyrase or topoisomerase IV	0.25	0.125
	Levofloxacin	LVX		1	0.25
	Moxifloxacin	MXF		2	0.5
Carbapenems	Imipenem	IPM	Binding to the penicillin-binding proteins	4	4
	Meropenem	MEM		0.5	1
Cephalosporins	Cefepime	FEP	Inhibiting penicillin-sensitive enzymes (transpeptidases, carboxypeptidases)	2	2
	Ceftazidime	CAZ		1	2
Penicillin	Temocillin	TMO	Inhibiting the transpeptidase that catalyzes the final step in cell wall biosynthesis	>64	>64
Glycopeptide	Vancomycin	VAN	Binding to the acyl-d-alanyl-d-alanine terminus of the growing peptidoglycan	>512	>512
Lipoglycopeptides	Telavancin	TEL	Inserting the lipophilic tail into the bacterial cell membrane causes rapid membrane depolarization and a potassium ion efflux	>512	>512
	Daptomycin	DAP		>512	>512
Rifamycin	Rifampicin	RIF	Inhibiting bacterial DNA-dependent RNA polymerase	16	16
Macrolide	Erythromycin	ERY	Binding to the 23S ribosomal RNA molecule in the 50S subunit of ribosomes	>64	>64
Aminocoumarin	Novobiocin	NVB	Inhibiting GyrB subunit of the bacterial DNA gyrase	>64	>64
Oxazolidinone	Linezolid	LZD	Binding a site on the bacterial 23S ribosomal RNA of the 50S subunit	0.5	1

(TEL, DAP), oxazolidinone (LZD), cephalosporins (FEP, CAZ), penicillin (TMO), fluoroquinolones (CIP, LVX, MOX), polymyxin (COL), aminoglycoside (AMK, GEN, TOB, NEO), an amphiphilic aminoglycoside (3',6-dinonyl neamine), carbapenems (IMI, MEM), rifamycin (RIF), macrolide (ERY), and aminocoumarin (NOV) (Table 2). Interestingly, fluoroquinolones have a MIC value lower (2-fold to 8-fold) against *P. aeruginosa*  $\Delta mlaA$  compared with WT, a decrease that was reversed in complemented strain. In contrast, no major change was observed for cephalosporins, polymyxin E, aminoglycoside (conventional or amphiphilic), and carbapenem. Also, antibiotics that were inefficient against *P. aeruginosa* WT, such as penicillin, glycopeptide, lipoglycopeptides, oxazolidinone, rifamycin, macrolide, and aminocoumarin, showed no decrease in MIC values in  $\Delta mlaA$  strain, suggesting that the sensitivity to antimicrobial compounds cannot be attributed to a global impairment of the OM/IM permeability. Changes in physicochemical parameters (i.e., hydrophobicity) could optimize the diffusion of some antibiotics, like fluoroquinolones, resulting in appropriate intracellular drug concentrations for antibacterial activity. A change in membrane fluidity might also impact the function of fluoroquinolone-specific efflux pumps or porins.

### Deletion of *mlaA* increased *P. aeruginosa* membrane vesiculation. 3',6-dinonyl neamine increased MVs number in WT and to a lesser extent in $\Delta mlaA$ strain

The differences in *P. aeruginosa* WT and  $\Delta mlaA$  concerning their membrane lipid composition (Fig. 1 and 2) as well as differences in Young's modulus (Fig. 3D) motivated us to investigate the formation of membrane-derived vesicles. The results showed that

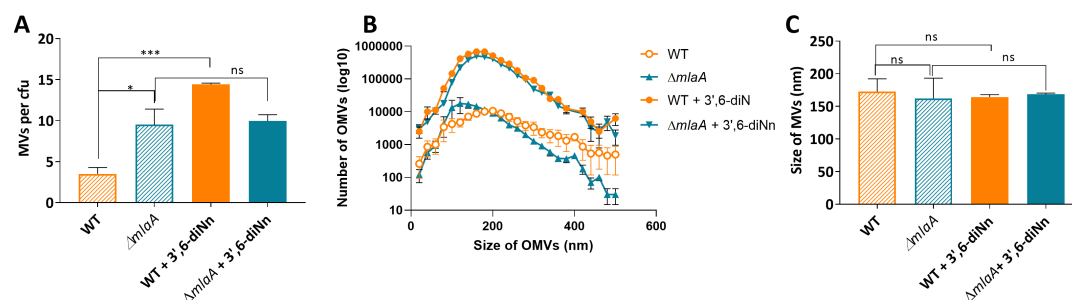


**FIG 7** MVs quantification. MVs *P. aeruginosa* WT and  $\Delta m1aA$  in the presence and absence of 3',6-dinonyl neamine ( $1\times$  MIC, 2 mg/L, 1 h) were analyzed using a nanoparticle tracking analyzer. (A) Number of MVs produced per colony forming unit (CFU). (B) MVs size distribution in nanometers (nm). Figure 6B was used to calculate the mean size of the membrane vesicles, which is shown in (C). Statistical analysis was performed by one-way ANOVA with Tukey's multiple-comparison test. \*\*\*\* $P < 0.0001$ , \*\* $P < 0.01$ , \* $P < 0.05$ ;  $^{ns}P > 0.05$ .

$\Delta m1aA$  produced more MVs (2.7-fold) compared with WT strain (Fig. 7A). This increase was largely reversed in complemented strain (Fig. S7B). The incubation of *P. aeruginosa* WT with 3',6-dinonyl neamine markedly increased the MVs production with an increase of 4.1-fold (Fig. 7A) with no effect on  $\Delta m1aA$ .

Regarding the MVs size distribution (Fig. 7B), no difference in the average mean size was observed when comparing MVs generated from WT ( $172.1 \pm 19.5$  nm) and  $\Delta m1aA$  ( $162.3 \pm 30.9$  nm) strains (Fig. 7C). The addition of 3',6-dinonyl neamine to WT ( $164.4 \pm 3.8$  nm) and  $\Delta m1aA$  ( $168.5 \pm 1.7$  nm) did not change mean size of MVs.

## DISCUSSION

The maintenance of OM lipid asymmetry is critical for resisting antibiotics and host stresses, as reported for numerous Gram-negative bacteria including *E. coli* (60), *H. influenzae* (61), *Burkholderia cepacia* complex structures (8), *A. baumannii* (62), and *P. aeruginosa* (10, 63). LPS levels and localization are involved in preserving the stiffness and permeability barrier of Gram-negative bacteria (64). As such, the Mla (maintenance of the OM lipid asymmetry) transport, composed of MlaA/VacJ-MlaCBDEF and facilitating the retrograde phospholipid transport from the outer back to the inner membrane (11), has been proposed as a target for drug development (14).

Here, we focused on MlaA, contributing to removing phospholipids from the outer leaflet of OM and transferring them to MlaC located in the periplasm. We explored the consequences of *m1aA* deletion on the mechanical (cell stiffness, turgor pressure), biophysical (surface charge, fluidity), and functional (MV generation, antibiotic susceptibility, permeability) properties of the OM in relation to changes in GPLs and LPS. All experiments were conducted in the absence and presence of one amphiphilic aminoglycoside, 3',6-dinonyl neamine, known to interact with *P. aeruginosa* OM, and especially with LPS and GPLs (29–31, 65).

First, the work shows the changes in membrane lipid composition induced by *P. aeruginosa* to defend against the deletion of *m1aA*. Total GPLs increased with a prominent effect on PE. In parallel, bacterial LPS levels decreased, and changes in lipid A structures (arabinylation, palmitoylation) were observed. These changes were associated with increased cell stiffness without alteration of turgor pressure and height profile. Remodeling of OM induced by *m1aA* deletion induced an increase in MVs generation without any significant effect on either IM fluidity or the IM/OM membrane permeability.

In the presence of 3',6-dinonyl neamine, *P. aeruginosa* WT also showed an increase in GPLs and a decrease in LPS with lipid A modifications (arabinylation and palmitoylation), but differences of *P. aeruginosa* WT and  $\Delta m1aA$  were observed with no significant effect on GPLs, a huge increase in LPS (associated with a decrease in lipid A hydroxylation and palmitoylation), decrease in cell stiffness and turgor pressure, and no effect on IM fluidity observed in  $\Delta m1aA$  strain. This might result in a slight and non-significant

increase in MVs generation and less permeabilization of the OM in  $\Delta mlaA$  as observed in WT strain. These differences of *P. aeruginosa* WT and  $\Delta mlaA$  in response to 3',6-dinonyl neamine might result not only from the extent of changes in GPLs and LPS contents but also from changes in lipid A structures, which may result in differences in drug lipid insertion.

At a glance, the study first highlighted how *P. aeruginosa* copes with *mlaA* deletion and modifies its membrane lipid composition. The data confirm a link between maintaining OM lipid asymmetry and regulating the level of LPS molecules at the surface of Gram-negative bacteria (11, 17, 60). Intriguingly, there is a decrease in LPS contents in  $\Delta mlaA$  compared with *P. aeruginosa* WT. The first hypothesis was the impact of *mlaA* deletion on LPS synthesis. We excluded a decrease in the stability of LpxC, one of the nine critical enzymes involved in lipid A synthesis, related to a partial or complete loss of YejM activity (64, 66, 67), since YejM was overexpressed in *P. aeruginosa*  $\Delta mlaA$  (Fig. S4A), in agreement with Guest and co-authors (64). Whether a decrease in lipid A synthesis could be afforded by a reduced LpxK activity induced by changes in the ratio of unsaturated and saturated fatty acids (68) or a competition for a common substrate for GPLs and LPS synthesis, that is,  $\beta$ -hydroxymyristoyl-ACP (69, 70), is unknown. We also ruled out a restriction of LPS transport to OM related to a decrease in CL synthesis (69, 71, 72) since we did not observe any major change in cardiolipin content in *P. aeruginosa*  $\Delta mlaA$  compared with WT (Fig. S3A). Finally, an increased release of LPS from the MVs in *P. aeruginosa*  $\Delta mlaA$  compared with WT must be also excluded (Fig. S8B).

Interestingly, LPS and GPLs varied in the opposite way. Since MVs are enriched in GPLs and not in LPS (Fig. S8A), they are unlikely involved in maintaining the ratio between LPS and GPLs. One other explanation could be changes in the directionality of phospholipid transport (from IM to OM-antegrade transport and from OM to IM-retrograde transport), even antegrade transport described for *A. baumannii* (62, 73) and *E. coli* (33), is largely disputed. For *P. aeruginosa*, to our knowledge, nothing has yet been published.

Beyond the effect induced by *mlaA* deletion on LPS levels and the ratio between LPS and GPLs, an effect on lysophospholipids was also observed with a higher LPG content compared with LPE. This could result (i) from a lack of activity of PldA and PagP toward PE, (ii) a higher stability of OM when PE flipped due to its zwitterionic character and small headgroup size (74), and (iii) a higher release of LPE in MVs derived from  $\Delta mlaA$  strain. In *P. aeruginosa* ATCC27853 WT and  $\Delta mlaA$ , PCR products of *pagP* and *pldA* were present (Fig. 2B; Fig. S4C). However, a significant increase in mRNA expression was observed only in the case of *pagP* (2.7-fold) (Fig. 2B; Fig. S4C).

Second, the consequences of *mlaA* deletion on the mechanical and biophysical properties of *P. aeruginosa* membranes were evidenced. *P. aeruginosa*  $\Delta mlaA$  showed an increase in cell surface stiffness likely linked with changes in lipid composition, including (i) longer acyl chains increasing the interactions between neighboring LPS molecules (3) and (ii) increase of phospholipids containing saturated acyl chains. However, the relationship between OM lipid composition and OM stiffness might be more complex, implying the presence of peptidoglycan and/or the link between peptidoglycan and OM (75, 76). Drugs interacting with LPS and/or GPLs like 3',6-dinonyl neamine also played a critical role in the mechanoproperties of bacterial membranes by decreasing cell stiffness and turgor pressure independently of the *mlaA* deletion or not. This could result from competition with  $Ca^{2+}$  and interaction with negatively-charged LPS, which could resolve the destabilization of the OM. No change was observed for the IM fluidity by comparing *P. aeruginosa*  $\Delta mlaA$  with WT, but a decrease of the surface charge was noticed, in agreement with lipid A modifications, including arabinosylation.

Third, focusing on the functional impact of *mlaA* deletion, a huge increase in the generation of MVs was observed in *P. aeruginosa*  $\Delta mlaA$ . This is in agreement with literature (77–80) and complements data reported on *Haemophilus influenzae*, *Vibrio cholera* (80), *Neisseria gonorrhoeae* (77), *Campylobacter jejuni* (79), and *E. coli* *mlaA* knockouts (81). Increased vesiculation might provide a transient advantage during the adaptation process. MlaA, by regulating vesiculation, could allow bacteria to spare the

consumption of energy requested by the continuous liberation of compounds of the OM and periplasm (80). The mechanism responsible for hypervesiculation in the  $\Delta mlaA$  strain is likely complex. Curvature inducing lipid molecules (negative and positive) at particular sites might favor MVs release from bacteria (34). Since we observed an increase in PE (Fig. S3A), which displays positive and negative intrinsic molecular curvatures, respectively (82–84), we could imagine the formation of highly curved structures such as membrane vesicles. However, other hypotheses might be raised like (i) weaker interactions between LPS molecules resulting from the insertion of GPLs into the outer leaflet of OM, favoring thus OM bulging and formation of vesicles (85), (ii) changes in thermotropic behavior and modifications of fluidity resulting from changes in unsaturated/saturated lipid acyl chain ratio (86, 87) or changes in the polar head may facilitate membrane vesiculation. The PE, PG, and CL ratio might be critical in this respect as the phase transition temperature ( $T_m$ ) of PE (DPPE, 41°C) is lower than that of PG (DPPG, 63°C). Also, CL is a lipid-containing four associated fatty acyl chains characterized by a high degree of unsaturation (88), which can form very rigid, gel-like membrane domains in the otherwise more fluid membrane promoting the initiation of vesicle formation (89). In addition, lipid A modifications resulting from environmental changes and PhoPQ-PmrAB activation (Fig. 2B), potentially interleaflet coupling with modified acylated lipid A and the pre-existing covalent linkages to peptidoglycans, could induce an increase of MVs production as reported for *Salmonella* (90). A last hypothesis is the accumulation of the PQS signaling molecule (2-heptyl-3-hydroxy-4-quinolone) in the outer leaflet of the OM. An increase in PQS was reported in *P. aeruginosa*  $\Delta mlaA$  compared with the WT (5), and this might promote OM curvature and vesiculation (91, 92). Besides these effects, MVs generation could also be influenced by changes in the covalent OM-peptidoglycan crosslinks resulting from integral proteins (i.e., Lpp) (93).

In the presence of 3,6-dinonyl neamine, a huge enhancement in the generation of MVs was noticed, especially for *P. aeruginosa* WT. Modulating the LPS biosynthesis, changes in lipid A structure might directly facilitate the formation of MVs or favor the insertion of the drug, promoting MVs generation (38, 94). The reduced effect on  $\Delta mlaA$  strains could be related to the lower content in LPS in comparison to WT or changes in lipid A modifications. This could be responsible for changes in the insertion of 3,6-dinonyl neamine into the outer leaflet of the OM with an increase in the surface area of the outer leaflet, leading to enhanced interleaflet tension that is relieved through induction of membrane curvature and subsequent MVs release. This agrees with mechanisms behind the MVs biogenesis that were previously described (82, 91).

In the end, the question of the potential impact on antibiotic susceptibility was raised. The reduced LPS levels in the  $\Delta mlaA$  strain were not sufficient to modify sensitivity to antibiotics like colistin or amphiphilic aminoglycoside, in agreement with the absence of OM permeabilization induced by these compounds at their MIC values. Two hypotheses could be raised (i) the decreased LPS may contribute to raise bacterial surface hydrophobicity, therefore, jeopardizing the outcome of *P. aeruginosa* interaction with hydrophobic and lipophilic molecules, and (ii) LPS modifications such as the lipid A palmitoylation and amino-arabinylation or aminoacylation of phospholipids as reported for *P. aeruginosa* (95, 96) may contribute to antimicrobial peptide resistance. These effects on LPS might explain why OM is less prone to be permeabilized in *P. aeruginosa*  $\Delta mlaA$  compared with WT strain impairing the activity of antibiotics like colistin for which the OM permeabilization is required to reach IM and induce cell lysis (97). More generally, if sensitivity to antimicrobial compounds is unlikely to be due to a global impairment of OM/IM permeability, changes in physicochemical parameters (i.e., hydrophobicity) could optimize the diffusion of some antibiotics such as fluoroquinolones. This could lead to appropriate intracellular drug concentrations for antibacterial activity. A change in membrane fluidity could also affect the function of fluoroquinolone-specific efflux pumps or porins.

Moving to the potential interest of MlaA in clinics, since this study does not consider the complexity of biological, clinically relevant conditions (98–100), it is difficult to

extrapolate our conclusions to the *in vivo* situation directly. Other *Pseudomonas* strains (PAO1, PA14) or clinical strains (from patients suffering from cystic fibrosis) should be selected. Especially, it would have been interesting to compare the *P. aeruginosa* clinical isolates from the different sites of infection and geographical areas to understand the role of MlaA in bacterial physiology and pathology in a healthcare setting. Interestingly, during lower respiratory tract infection in non-typeable *H. influenzae* (NTHi) modulation of outer leaflet of OM through increased expression of *mlaA* (*vacJ*) genes could minimize recognition by bactericidal anti-oligosaccharide antibodies (61).

In conclusion, this work highlights some aspects of the membrane dynamics of *P. aeruginosa*: (i) the cross-talk between LPS and glycerophospholipids mislocated at the outer leaflet of the OM of *P. aeruginosa* (34) and (ii) the role of the individual glycerophospholipids and lipid A structures for changes in mechanical properties of OM, including cell stiffness, turgor pressure, and IM fluidity. The impact of the changes in membrane lipid composition on biophysical and functional membrane properties, including vesiculation and permeability, was also assessed. Although it is risky to define mechanical hypotheses linking lipid composition and membrane biophysical properties, especially since the system maintaining OM asymmetry is complex and involves several proteins probably acting in a coordinated manner, a better understanding of membrane biophysics as the maintenance of OM lipid asymmetry in link with lipid membrane composition is a pre-requisite for opening new research avenues in the design of innovative antibacterial drugs.

## MATERIALS AND METHODS

3',6-dinonyl neamine (3',6-diNn) was synthesized by Decout and colleagues (101). *P. aeruginosa* strain ATCC27853 (WT) was obtained from the Pasteur Institute (Brussels, Belgium; Prof. R. Vanhoof). Muller-Hinton broth cation-adjusted (MHB-Ca) and Luria-Bertani broth (LB) were purchased from Roth™. LPE-17:1, LPG-17:1, and CL-14:0, used as internal standards, were purchased from Avanti Polar Lipids. FAME standards were ordered from Larodan (Solna, Sweden). CH<sub>3</sub>CN, CHCl<sub>3</sub>, CH<sub>3</sub>OH, and hexane from Fisher Scientific (Leicestershire, UK) were of high-performance liquid chromatography (HPLC) grade and were used without further purification. All other reagents and chemicals used were of the highest grade of purity commercially available. Milli-Q H<sub>2</sub>O was filtered through a 0.22 μm filter and obtained using a Milli-Q Millipore system (Milli-Q plus 185).

### Bacterial strains and culture conditions

Strains were grown on Tryptic Soy Agar (TSA), Luria-Bertani (LB) agar plates, or in LB media. *P. aeruginosa*  $\Delta mlaA$  (PA\_2800) mutant was created using two-step allelic exchange (102–104) as described earlier (5). Complementation was carried out to ensure that the deletion of the *mlaA* gene did not have a polar effect on adjacent genes or mutations elsewhere in the genome during the construction process. Wild-type *mlaA* under the control of its native promoter (*PmlaA*) was cloned into the mini-Tn7 vector, which was then used to integrate a single copy of *PmlaA-mlaA* at the *attTn7* site into the chromosome of *P. aeruginosa* ATCC27853  $\Delta mlaA$  by transposition as previously described in Choi and Schweizer (105).

*P. aeruginosa* ATCC27853 and *P. aeruginosa*  $\Delta mlaA$  strains grew until the mid-exponential phase. For some experiments, strains were then incubated with 3',6-dinonyl neamine at its MIC (2 μg/mL) against *P. aeruginosa* for 1 h.

Some of the phenotypes with complemented strains ( $\Delta mlaA$  *att7::mmlaA*) were characterized and found to be similar to those from WT for growth rate, PQS levels, motility including swarming, swimming and twitching (5), or MVs generation and MICs (this study).

## Quantitative reverse transcription-polymerase chain reaction (RT-qPCR)

RT-qPCR was done to quantify the mRNA transcripts from the WT, the  $\Delta mlaA$ , and the  $\Delta mla\ att7::mlaA$ . Total RNA was isolated using InviTrap Spin Universal RNA Minit Kit (INVITEK). DNA contamination was removed by TURBO DNA-free™ kit from Invitrogen, and RNA was quantified using nanodrop (OD<sub>260</sub>). One microgram of total RNA was heated at 65°C for 15 min and then cooled down at 0°C, mixed with buffer, MgCl<sub>2</sub>, random hexamers, dNTP mix, RNase inhibitor, and reverse transcriptase to synthesize complementary DNA (cDNA) using first-strand cDNA synthesis Kit (ref 11483188001, Roche). Reverse transcription was performed on iCyclerIQ (BIO-RAD) with thermal cycler programming as follows: 25°C for 10 min; 42°C for 60 min; 99°C for 5 min, and 4°C for 5 min. Real-time PCR was performed with SYBR green (SsoAdvanced Universal SYBR Green Supermix, BIO-RAD) and using the primers specified in Table S1 using a CF96 Real-Time System (C1000 Touch Thermal cycler, BIO-RAD).

## Lipid analysis

The lipid content of the different samples was analyzed by LC-MS, as previously reported (56). Briefly, lipids from the membranes were analyzed after liquid/liquid extraction (CH<sub>2</sub>Cl<sub>2</sub>-CH<sub>3</sub>OH-H<sub>2</sub>O, 4:2:1, vol/vol/vol) under an acidic condition in the presence of internal standards (LPE-17:1, LPG-17:1, and CL-14:0). Phospholipid analysis was performed using a Xevo TQ-S (Waters, USA), and cardiolipin analysis was carried out on an LTQ-orbitrap (from Thermo Fisher Scientific).

For the phospholipids, an HSS LC-18 column 100 × 2.1 mm, 1.8 μm (Waters, USA) was used at a temperature of 40°C. The mobile phase consisted of a gradient between A: CH<sub>3</sub>OH-CH<sub>3</sub>CN (9:1, vol/vol) 75% H<sub>2</sub>O 25%; B: CH<sub>3</sub>OH-CH<sub>3</sub>CN (9:1, vol/vol) and C: CH<sub>3</sub>(CH<sub>2</sub>)<sub>2</sub>-2-OH, all containing ammonium acetate (5 mM). An ESI probe, operated in negative mode, was used for sample ionization. The mass spectrometer parameters were as follows: capillary voltage: 2.9kV; cone voltage: 70V; desolvation temperature: 400°C; desolvation gas flow: 1,000 L/h; cone gas flow: 150 L/h; and nebulizer: six bars.

For the analysis of cardiolipins, a Nucleosil C8 column 150 × 4 mm, 5 μm (Macherey-Nagel, GmbH & Co. KG) was used. The same mobile phase as used for the other phospholipids was selected. An ESI probe operated in negative mode was used for cardiolipin ionization. The mass spectrometer parameters were as follows: capillary voltage: -40V; capillary temperature: 275°C; tube lens voltage: -173V; sheath gas flow: 20AU; auxiliary gas flow: 10AU, and sweep gas flow: 8AU.

The relative quantification of the lipids was based on the ratio between the area under the curve (AUC) of the lipid structures and the AUC of the respective internal standard. The obtained data were normalized to the total lipid content determined via labeling the lipids with FM4-64.

## Lipopolysaccharides (LPS) extraction and quantification

To quantify LPS levels, LPS molecules were extracted from bacterial suspensions at mid-log growth phases and quantified by purpald assay, with data normalized to colony-forming units.

LPS was extracted from bacteria using an LPS extraction kit (iNtRON Biotechnology). Briefly, *P. aeruginosa* cells were harvested at 2978 g for 5 min. One milliliter of lysis buffer was added to the pellet and vortexed vigorously. Two hundred microliters of CHCl<sub>3</sub> were added to the suspension, vortexed, and incubated at room temperature for 5 min. The suspension was centrifuged to pipette out the upper layer (400 μL). Eight hundred microliters of purification buffer were mixed, and LPS was precipitated by incubation at -20°C for 20 min. After centrifugation, the LPS pellet was washed with 70% ethanol and dissolved in 10 mM Tris-HCl. Samples were then lyophilized to get powder until further use.

LPS was quantified using purpald assay based on periodate oxidation of formaldehyde generated from 2-keto-3-deoxyoctonate (KDO) (106, 107). Briefly, 50 μL of LPS



samples or standards (LPS from *P. aeruginosa* serotype 10, 0–1,200 µg/mL) was added to 50 µL of 32 mM NaIO<sub>4</sub> in a 96-well plate and incubated for 25 min. Fifty microliters of 136 mM purpald reagent in 2 N NaOH were added to each well, followed by incubation for 20 min, and the addition of 50 µL of 64 mM NaIO<sub>4</sub>. After 20 min of incubation, absorbance was measured at 550 nm with a SpectraMax M3 microplate reader (Molecular Devices, Sunnyvale, CA, USA).

By using standard curve for quantification (determined for each independent assay), and for sake of comparison, the results are expressed in %. We considered as 100%, the value obtained for *P. aeruginosa* WT and untreated and the values obtained for  $\Delta mlaA$  strain and for WT/ $\Delta mlaA$  *P. aeruginosa* treated with 3',6-dinonyl neamine or colistin were compared to this value (100%).

### Lipid A sample preparation and analysis

From LPS extracts, lipid A samples were prepared by mild hydrolysis with 200 µL 1% acetic acid at 100°C for 2 h (108). The solution was left at room temperature to cool down, and 400 µL of CHCl<sub>3</sub> and 200 µL of H<sub>2</sub>O were added. The solution was then centrifuged to obtain a bottom layer that was dried under N<sub>2</sub> stream. Lipid A samples were resuspended in CHCl<sub>3</sub>:CH<sub>3</sub>OH (4:1, vol/vol) and analyzed by direct injection with an LTQ-orbitrap mass spectrometer (Thermo Fisher Scientific, Bleiswijk, The Netherlands) in negative mode with electrospray ionization. The samples were directly infused at a flow rate of 10 µL/min for 3 min. The MS conditions were: capillary temperature: 275°C, capillary voltage: –10 V, and tube lens: –125 V. Sheath gas, auxiliary gas, and sweep gas flow rates were set at 5 AU.

### Fatty acid extraction from lipid A and analysis

The lipid A extract was treated according to a procedure adapted from Myron Sasser (109). Briefly, after adding the internal standard C20:0 (Larodan, Solna, Sweden), the extract was saponified by adding NaOH, CH<sub>3</sub>OH, and water. The methylation of fatty acids was done by adding HCl, water, and CH<sub>3</sub>OH to the solution. FAMES were extracted using a mixture of hexane and methyl tert-butyl ether (1/1; vol/vol). Before injection in gas chromatography, the extract (hexane, methyl tert-butyl ether) was purified by adding water and sodium hydroxide.

FAMES were injected and separated by gas chromatography (GC) (Trace 2000; Thermo Finnigan, Milan, Italy) equipped with an autosampler (GC PAL, CTC Analytics, Zwingen, Switzerland) and a column Ultra 2 (25 m × 0.32 mm ID, film thickness 0.52 µm; Agilent Technologies, Santa Clara, CA, USA), continuously flowed with H<sub>2</sub> as a carrier gas at a constant pressure of 60 kPa. The GC temperature program was the following: an initial temperature of 80°C, which increased to 170°C with a temperature slope of 25°C/min, then from 170°C to 300°C with a slope of 5°C/min. The temperature of 300°C was maintained for 2 min to clean the column. FAMES were detected with flame ionization detector (Thermo Finnigan, Milan, Italy) kept at a constant temperature of 255°C and flowed by air (350 mL/min) and H<sub>2</sub> (35 mL/min). An external standard composed of FAME C10:0, 3OH-C10:0, C12:0, 2OH-C12:0, 3OH-C12:0, C16:0, and C20:0 (Larodan, Solna, Sweden) was used to identify the unknown peaks with the retention time and quantify the peaks through the known concentrations. Chromatographs were processed by using ChromQuest 5.0 software (Thermo Finnigan, Milan, Italy). The results were normalized with the total LPS amount and expressed in µg.

### MVs isolation and characterization

*P. aeruginosa* WT and  $\Delta mlaA$  strains were grown in one-fifth of the volume of Erlenmeyer's flasks until mid-logarithmic phase and treated with 3', 6-dinonyl neamine (1× MIC, 2 µg/mL) for 1 h. The bacterial cells were pelleted by centrifugation at 2,978 g at 4°C (Eppendorf 5810 R centrifuge: A-4–62 rotor). The supernatant was filtered via a 0.45 µm polyvinylidene difluoride (PVDF) filter (Whatman) and then ultracentrifuged at 150,000 g for

3 h at 4°C (Beckman™; 80 Ti rotor). The supernatant was discarded, and the pellet was resuspended in 10 mM HEPES-0.85% NaCl buffer, pH7.2 (MVs buffer). The MVs were purified using gradient density of OptiPrep-iodixanol (Sigma-Aldrich) in MV buffer, as described previously (110). ZetaVIEW S/N 18–400 (x30 series, Inning am Ammersee, Germany) was used to determine the size distribution and the amount of the MVs.

### Outer membrane isolation

Outer membrane from *P. aeruginosa* WT and  $\Delta mlaA$ , non-treated and treated with 3',6-dinonyl neamine, was extracted using Mizuno and Kageyama's protocol (111). Briefly, bacteria were grown in LB media at 37°C, until OD<sub>620</sub>: 0.8. Cell pellet (1.5 g) was suspended in 9 mL of 2 M sucrose, 10 mL of 0.1 M Tris-HCl (pH 7.8 at 25°C), 0.8 mL of 1% Na-EDTA (ethylenediaminetetraacetic acid disodium salt) (pH 7.0), and 1.8 mL of 0.5% lysozyme and incubated at 37°C for 60 min. After 30 min of incubation, DNase (3 µg/mL) was added, and incubation was continued for a further 30 min. Samples were centrifuged at 15,000 g, for 15 min, at 37°C to remove the spheroplasts. The supernatant was ultracentrifuged at 100,000 g, 60 min, 4°C to recover the outer membranes. Total lipids and proteins were quantified with a fluorescent probe FM4-64 and BCA protein assay kit (Pierce, ThermoFisher), respectively.

The absence of IM as a contaminant was confirmed with NADH oxidase assay, an IM-specific enzyme. Upon time, OM extracted from *P. aeruginosa* WT strain showed no change in absorbance, whereas IM extracts from *P. aeruginosa* and *E. coli* decreased in absorbance reflecting NADH consumption (Fig. S1A). To further confirm the absence of IM, western blot against LepB, an IM protein, was performed using IM extracted from *E. coli* as a positive control. The WB did not show any band in OM of *P. aeruginosa*, whereas IM showed the presence of LepB (Fig. S1B).

### Atomic force microscopy (AFM)

#### Bacterial growth conditions

*P. aeruginosa* WT and  $\Delta mlaA$  cells were cultured overnight in 10 mL of LB medium, at 37°C, under shaking. Stationary phase cultures were then diluted to an OD<sub>600</sub> = 0.1 in the same culture medium and allowed to grow until the exponential phase (OD<sub>600</sub> = 0.8) under shaking at 37°C. *P. aeruginosa* WT and  $\Delta mlaA$  strains were treated with 1× MIC (2 µg/mL) 3',6-dinonyl neamine for 1 h. The cells were then centrifuged (2,000 g, 5 min), washed and resuspended in 1× PBS. These washing and resuspension steps were repeated twice, and at the end, the cellular suspension was diluted 1:100 in PBS.

#### Sample preparation

AFM studies were conducted with bacteria immobilized on glass-bottom Petri dishes previously coated with Poly-L-Lysine (PLL). PLL coating was achieved by letting the dish in contact with PLL solution for 20 min at room temperature and after rinsing twice with PBS to remove non-attached PLL molecules. One milliliter of bacterial suspension was subsequently added to the PLL-coated dish and incubated for 20 min at room temperature. After that, at least three rinsing steps with PBS were performed, and the dish was filled with 2 mL of this buffer.

#### AFM imaging and mechanical studies

Both imaging and mechanical studies were carried out with MSCT-C cantilevers (Bruker), in PBS, at room temperature, using a JPK NanoWizard 4 NanoScience AFM. Before the experiments, the cantilevers were thoroughly rinsed with water and ethanol, dried with N<sub>2</sub> flow, and further cleaned in a UV ozone chamber for 15 min. Freshly cleaned cantilevers were calibrated by the thermal noise method (112), and spring constant values were found to be always approximately 0.02 N m<sup>-1</sup>. Bacteria were first imaged in quantitative imaging (QI) mode at 128 × 128 pixels resolution, using an applied

force of 0.5 nN, a constant approach/retract speed of 30  $\mu\text{m/s}$ , and a ramp size of 500 nm. High-resolution (256  $\times$  256 pixels) QI images were then recorded by imaging a 400  $\times$  400  $\text{nm}^2$  area on top of the bacteria, keeping the same imaging parameters. Mechanical measurements were conducted in force volume (FV) mode. For each cell, 256 force-distance curves (16  $\times$  16 pixels) were recorded on 250  $\times$  250  $\text{nm}^2$  areas using an applied force of 1 nN, a constant approach/retract speed of 1  $\mu\text{m/s}$ , and a ramp size of 1  $\mu\text{m}$ . Data were analyzed with the JPK Data Processing software (version 6.1.172). The approach segment of the force-distance curves was fitted with the Hertz/Sneddon model over a distance of 20 nm, using a Poisson ratio of 0.5 and considering a conical tip of 15° half-cone angle (113). Although the Young's Modulus ( $E$ ) was extracted from the nonlinear region of the curves, the spring constant ( $k$ ) was calculated through the slope of their linear region.

## Fluorescence-lifetime imaging microscopy (FLIM)

### Sample preparation

*BODIPY-C10* was obtained from the Molecular Design and Synthesis lab at KU Leuven. The bacterial slide preparation protocol was adapted from previous studies with some modifications (56, 114). Briefly, the cells ( $10^7$  CFU/mL) were resuspended in the PBS containing BODIPY-C10 (0.5  $\mu\text{M}$ ) supplemented with 0.1% wt/vol of glucose. The cells were labeled by mixing and incubating at 37°C with shaking. Subsequently, 200  $\mu\text{L}$  of the cell suspensions was immobilized on the 8-well Ibidi microscopy chamber, precoated with 0.01% poly-L-Lysine. BODIPY-C10 concentrates mostly in the inner membrane of *P. aeruginosa* (56).

### FLIM imaging

The chambers containing the bacteria were mounted on a confocal & multiphoton microscope (LSM 980, ZEISS) equipped with a time-correlated single photon counting (TCSPC) system FLIM module (PicoQuant, Germany). BODIPY-C10 was excited with a coherent (Chameleon Discovery) pulsed laser (80 MHz) at 800 nm, and emission was recorded over a spectrum of 505–545 nm. The FLIM images were obtained at the resolution of 512  $\times$  512 pixels.

The analysis of the FLIM images was performed with SymPhoTime 64 software, which allows fitting the fluorescence decay of the images' pixels to mathematical decay models. An average lifetime is hence calculated for each pixel, which is color-coded in the FLIM images. Each decay curve and its corresponding image were acquired after collecting 1,000 photons.

## Membrane permeabilization by 3', 6-dinonyl neamine

### OM permeabilization

The OM permeabilization was assessed by the method used by Angus et al (115). Briefly, the overnight culture of *P. aeruginosa* was grown. 0.25  $\mu\text{g/mL}$  of imipenem was added to the bacterial culture to induce a higher level of  $\beta$ -lactamases and incubated for an hour. Bacteria were centrifuged at 3,000 g for 7 min and then, resuspended in 1 $\times$  PBS (pH 7.2) to get an OD<sub>620</sub> 0.5. Thereafter, 50  $\mu\text{L}$  of different concentrations (0–10  $\mu\text{M}$ ) of 3', 6-dinonyl neamine was added to 100  $\mu\text{L}$  bacterial suspension. Fifty microliters of nitrocefin (50  $\mu\text{g/mL}$ ) were added in the 96-well plates. Absorbance at 490 nm was monitored with a SpectraMax M3 microplate reader at 25°C (Molecular Devices, Sunnyvale, CA, USA). Ten micrometers of colistin was used as a positive control (100%).

### IM permeability

The permeabilization of bacterial membranes was determined by using a membrane-impermeable probe, propidium iodide (PI), which fluoresces only when it binds to DNA

(31). Briefly, an overnight culture of *P. aeruginosa* was grown and diluted to ( $OD_{620}$  0.5) and added to PI (dissolved in water) and different concentrations of 3',6'-dinyonyl neamine (0–10  $\mu$ M). Suspension was incubated in dark for 15 min, and fluorescence intensity for excitation, 540 nm, and emission, 610 nm, was measured with a SpectraMax M3 microplate reader at 25°C (Molecular Devices, Sunnyvale, CA, USA). Ten micrometers of colistin were used as a positive control (100%).

### Antibiotic susceptibility assay

MICs of antibiotics were assessed by microdilution in cation-adjusted-Mueller Hinton Broth according to Clinical and Laboratory Standard Institute (2018).

### Zeta potential

Dynamic light scattering (DLS) technology was performed using a Zetasizer Nano SZ equipment from Malvern Instruments (Grovedwood Road, UK) with patented NIBS (non-invasive back scatter) technology, and the recommended software was used for zeta potential determination.

### ACKNOWLEDGMENTS

The authors wish to thank Prof. Wim Dehaen and Dr. Tomas Opsomer for providing us with the BODIPY-C10 probe, Virginie Mohymont and Romain Tricot for providing dedicated technical assistance.

This work was supported by the F.S.R-FNRS, T.1003.14, J.0205.16, T.0175.20, and by UCL (ARC 17.22.085; Study Grants Covid [2022] and Patrimoine [2023]).

### AUTHOR AFFILIATIONS

<sup>1</sup>UCLouvain, Louvain Drug Research Institute, Cellular & Molecular Pharmacology, Brussels, Belgium

<sup>2</sup>UCLouvain, Louvain Institute of Biomolecular Science and Technology, nanoBiophysics, Louvain-la-Neuve, Belgium

<sup>3</sup>UCLouvain, Louvain Drug Research Institute, Pharmacognosy, Brussels, Belgium

<sup>4</sup>UCLouvain, Louvain Drug Research Institute, Bioanalysis and Pharmacology of Bioactive Lipids, Brussels, Belgium

<sup>5</sup>UCLouvain, Louvain Institute of Biomolecular Science and Technology, Biochemistry of Nutrition and Environmental Toxicology Louvain-la-Neuve, Brussels, Belgium

<sup>6</sup>Université Grenoble Alpes, CNRS, DPM, Grenoble, France

### AUTHOR ORCIDs

N. Mozaheb  <http://orcid.org/0000-0001-6259-9512>

M.-P. Mingeot-Leclercq  <http://orcid.org/0000-0002-2569-2619>

### FUNDING

Funder	Grant(s)	Author(s)
Fonds De La Recherche Scientifique - FNRS (FNRS)	T.0175.20	M.-P. Mingeot-Leclercq
AUL   Université Catholique de Louvain (UCL)	17.22.085	M.-P. Mingeot-Leclercq
AUL   Université Catholique de Louvain (UCL)	Patrimoine	M.-P. Mingeot-Leclercq
AUL   Université Catholique de Louvain (UCL)	Covid	M.-P. Mingeot-Leclercq

### AUTHOR CONTRIBUTIONS

M. Kaur, Data curation, Formal analysis, Investigation, Methodology, Writing – original draft, Writing – review and editing | N. Mozaheb, Data curation, Formal analysis,

Investigation, Methodology, Writing – original draft | T. O. Paiva, Data curation, Formal analysis, Investigation, Methodology, Writing – original draft | M.-F. Herent, Conceptualization, Data curation, Formal analysis, Investigation, Methodology, Writing – original draft | F. Goormaghtigh, Conceptualization, Investigation, Validation | A. Paquot, Data curation, Formal analysis, Investigation, Methodology, Writing – original draft | R. Terrasi, Conceptualization, Data curation, Formal analysis, Investigation, Methodology, Writing – original draft | E. Mignolet, Data curation, Formal analysis, Investigation, Methodology, Writing – original draft | J.-L. Décout, Conceptualization, Data curation, Formal analysis, Investigation, Methodology, Writing – original draft | J. H. Lorent, Writing – review and editing | Y. Larondelle, Formal analysis, Methodology, Writing – original draft | G. G. Muccioli, Formal analysis, Methodology, Writing – original draft | J. Quetin-Leclercq, Formal analysis, Methodology, Writing – original draft | Y. F. Dufrière, Conceptualization, Formal analysis, Methodology, Writing – original draft | M.-P. Mingeot-Leclercq, Conceptualization, Funding acquisition, Methodology, Project administration, Resources, Supervision, Validation, Writing – original draft, Writing – review and editing

## ADDITIONAL FILES

The following material is available [online](#).

### Supplemental Material

**Figure S1 (Spectrum01484-24-s0001.tiff).** (A) NADH oxidase activity upon time; (B)Western Blot; (C)PCR products of *mlaA*, *mlaB*, *mlaC*, *mlaD*, *mlaE*, and *mlaF*; (D)Relative mRNA expression in the  $\Delta mlaA$  strain.

**Figure S2 (Spectrum01484-24-s0002.tiff).** Individual glycerophospholipids (PE, PG, CL) and lysophospholipids (LPE, LPG) species analysis.

**Figure S3 (Spectrum01484-24-s0003.tiff).** (A) Individual glycerophospholipids; (B) lysophosphoglycerides; (C) and saturated, monounsaturated, and polyunsaturated fatty acyl chains.

**Figure S4 (Spectrum01484-24-s0004.tiff).** mRNA expression.

**Figure S5 (Spectrum01484-24-s0005.tiff).** AFM height characterization of *P. aeruginosa* WT and  $\Delta mlaA$  non-treated and treated.

**Figure S6 (Spectrum01484-24-s0006.tif).** Zeta potential of the bacterial envelope of *P. aeruginosa* WT and  $\Delta mlaA$  strains.

**Figure S7 (Spectrum01484-24-s0007.tif).** Membrane vesicles (MVs) quantification.

**Figure S8 (Spectrum01484-24-s0008.tif).** Composition of Membrane vesicles (MVs) (n=3) with (A) GPLs and (B) LPS.

**Tables S1 to S3 (Spectrum01484-24-s0009.docx).** Table S1: Primers used. Table S2: Predicted lipid A acyl chains. Table S3: Relative intensity of lipid A structures.

**Supplemental material (Spectrum01484-24-s0010.docx).** Supplemental captions of figures and tables, and additional experimental details.

## REFERENCES

- Kondakova T, D'Heygère F, Feuilloley MJ, Orange N, Heipieper HJ, Duclairoir Poc C. 2015. Glycerophospholipid synthesis and functions in *Pseudomonas*. *Chem Phys Lipids* 190:27–42. <https://doi.org/10.1016/j.chemphyslip.2015.06.006>
- Henderson JC, Zimmerman SM, Crofts AA, Boll JM, Kuhns LG, Herrera CM, Trent MS. 2016. The power of asymmetry: architecture and assembly of the Gram-negative outer membrane lipid bilayer. *Annu Rev Microbiol* 70:255–278. <https://doi.org/10.1146/annurev-micro-102215-095308>
- Nikaido H. 2003. Molecular basis of bacterial outer membrane permeability revisited. *Microbiol Mol Biol Rev* 67:593–656. <https://doi.org/10.1128/MMBR.67.4.593-656.2003>
- Carpenter CD, Cooley BJ, Needham BD, Fisher CR, Trent MS, Gordon V, Payne SM. 2014. The Vps/VacJ ABC transporter is required for intercellular spread of *Shigella flexneri*. *Infect Immun* 82:660–669. <https://doi.org/10.1128/IAI.01057-13>
- Kaur M, Buyck JM, Goormaghtigh F, Decout J-L, Mozaheb N, Mingeot-Leclercq M-P. 2023. Deficient *Pseudomonas aeruginosa* in MlaA/VacJ outer membrane lipoprotein shows decrease in rhamnolipids secretion, motility, and biofilm formation, and increase in fluoroquinolones susceptibility and innate immune response. *Res Microbiol* 174:104132. <https://doi.org/10.1016/j.resmic.2023.104132>
- Suzuki T, Murai T, Fukuda I, Tobe T, Yoshikawa M, Sasakawa C. 1994. Identification and characterization of a chromosomal virulence gene, *vacJ*, required for intercellular spreading of *Shigella flexneri*. *Mol Microbiol* 11:31–41. <https://doi.org/10.1111/j.1365-2958.1994.tb00287.x>
- Zhao L, Gao X, Liu C, Lv X, Jiang N, Zheng S. 2017. Deletion of the *vacJ* gene affects the biology and virulence in *Haemophilus parasuis* serovar 5. *Gene* 603:42–53. <https://doi.org/10.1016/j.gene.2016.12.009>
- Bernier SP, Son S, Surette MG. 2018. The Mla pathway plays an essential role in the intrinsic resistance of *Burkholderia cepacia* complex species

- to antimicrobials and host innate components. *J Bacteriol* 200:e00156-18. <https://doi.org/10.1128/JB.00156-18>
9. McDaniel C, Su S, Panmanee W, Lau GW, Browne T, Cox K, Paul AT, Ko SHB, Mortensen JE, Lam JS, Muruve DA, Hassett DJ. 2016. A putative ABC transporter permease is necessary for resistance to acidified nitrite and EDTA in *Pseudomonas aeruginosa* under aerobic and anaerobic planktonic and biofilm conditions. *Front Microbiol* 7. <https://doi.org/10.3389/fmicb.2016.00291>
  10. Munguia J, LaRock DL, Tsunemoto H, Olson J, Cornax I, Pogliano J, Nizet V. 2017. The Mla pathway is critical for *Pseudomonas aeruginosa* resistance to outer membrane permeabilization and host innate immune clearance. *J Mol Med* 95:1127–1136. <https://doi.org/10.1007/s00109-017-1579-4>
  11. Malinverni JC, Silhavy TJ. 2009. An ABC transport system that maintains lipid asymmetry in the Gram-negative outer membrane. *Proc Natl Acad Sci U S A* 106:8009–8014. <https://doi.org/10.1073/pnas.0903229106>
  12. Abellón-Ruiz J, Kaptan SS, Baslé A, Claudi B, Bumann D, Kleinekathöfer U, van den Berg B. 2017. Structural basis for maintenance of bacterial outer membrane lipid asymmetry. *Nat Microbiol* 2:1616–1623. <https://doi.org/10.1038/s41564-017-0046-x>
  13. Ekiert DC, Bhabha G, Isom GL, Greenan G, Ovchinnikov S, Henderson IR, Cox JS, Vale RD. 2017. Architectures of lipid transport systems for the bacterial outer membrane. *Cell* 169:273–285. <https://doi.org/10.1016/j.cell.2017.03.019>
  14. Huang Y-MM, Miao Y, Munguia J, Lin L, Nizet V, McCammon JA. 2016. Molecular dynamic study of MlaC protein in Gram-negative bacteria: conformational flexibility, solvent effect and protein-phospholipid binding. *Protein Sci* 25:1430–1437. <https://doi.org/10.1002/pro.2939>
  15. Tang X, Chang S, Qiao W, Luo Q, Chen Y, Jia Z, Coleman J, Zhang K, Wang T, Zhang Z, Zhang C, Zhu X, Wei X, Dong C, Zhang X, Dong H. 2021. Structural insights into outer membrane asymmetry maintenance in Gram-negative bacteria by MlaFEDB. *Nat Struct Mol Biol* 28:81–91. <https://doi.org/10.1038/s41594-020-00532-y>
  16. Thong S, Ercan B, Torta F, Fong ZY, Wong HYA, Wenk MR, Chng S-S. 2016. Defining key roles for auxiliary proteins in an ABC transporter that maintains bacterial outer membrane lipid asymmetry. *Elife* 5:1–19. <https://doi.org/10.7554/eLife.19042>
  17. May KL, Silhavy TJ. 2018. The *Escherichia coli* phospholipase PldA regulates outer membrane homeostasis via lipid signaling. *MBio* 9:1–14. <https://doi.org/10.1128/mBio.00379-18>
  18. Powers MJ, Trent MS. 2018. Expanding the paradigm for the outer membrane: *Acinetobacter baumannii* in the absence of endotoxin. *Mol Microbiol* 107:47–56. <https://doi.org/10.1111/mmi.13872>
  19. Ahn VE, Lo EI, Engel CK, Chen L, Hwang PM, Kay LE, Bishop RE, Privé GG. 2004. A hydrocarbon ruler measures palmitate in the enzymatic acylation of endotoxin. *EMBO J* 23:2931–2941. <https://doi.org/10.1038/sj.emboj.7600320>
  20. Filkin SY, Lipkin AV, Fedorov AN. 2020. Phospholipase superfamily: structure, functions, and biotechnological applications. *Biochemistry (Mosc)* 85:S177–S195. <https://doi.org/10.1134/S0006297920140096>
  21. Bishop RE. 2008. Structural biology of membrane-intrinsic  $\beta$ -barrel enzymes: sentinels of the bacterial outer membrane. *Biochim et Biophys Acta (BBA) - Biomembranes* 1778:1881–1896. <https://doi.org/10.1016/j.bbamem.2007.07.021>
  22. Dekker N. 2000. Outer-membrane phospholipase A: known structure, unknown biological function. *Mol Microbiol* 35:711–717. <https://doi.org/10.1046/j.1365-2958.2000.01775.x>
  23. Snijder HJ, Ubarretxena-Belandia I, Blaauw M, Kalk KH, Verheij HM, Egmond MR, Dekker N, Dijkstra BW. 1999. Structural evidence for dimerization-regulated activation of an integral membrane phospholipase. *Nature New Biol* 401:717–721. <https://doi.org/10.1038/44890>
  24. Sun L, Zhang Y, Cai T, Li X, Li N, Xie Z, Yang F, You X. 2022. CrrAB regulates PagP-mediated glycerophosphoglycerol palmitoylation in the outer membrane of *Klebsiella pneumoniae*. *J Lipid Res* 63:100251. <https://doi.org/10.1016/j.jlcr.2022.100251>
  25. Tam C, Missiakas D. 2005. Changes in lipopolysaccharide structure induce the  $\sigma^E$ -dependent response of *Escherichia coli*. *Mol Microbiol* 55:1403–1412. <https://doi.org/10.1111/j.1365-2958.2005.04497.x>
  26. Jia W, El Zoeiby A, Petruzzello TN, Jayabalasingham B, Seyedirashiti S, Bishop RE. 2004. Lipid trafficking controls endotoxin acylation in outer membranes of *Escherichia coli*. *J Biol Chem* 279:44966–44975. <https://doi.org/10.1074/jbc.M404963200>
  27. Wu T, McCandlish AC, Gronenberg LS, Chng S-S, Silhavy TJ, Kahne D. 2006. Identification of a protein complex that assembles lipopolysaccharide in the outer membrane of *Escherichia coli*. *Proc Natl Acad Sci U S A* 103:11754–11759. <https://doi.org/10.1073/pnas.0604744103>
  28. Dalebroux ZD, Matamouros S, Whittington D, Bishop RE, Miller SI. 2014. PhoPQ regulates acidic glycerophospholipid content of the *Salmonella typhimurium* outer membrane. *Proc Natl Acad Sci USA* 111:1963–1968. <https://doi.org/10.1073/pnas.1316901111>
  29. Sautrey G, Zimmermann L, Deleu M, Delbar A, Souza Machado L, Jeannot K, Van Bambeke F, Buyck JM, Decout J-L, Mingeot-Leclercq M-P. 2014. New amphiphilic neamine derivatives active against resistant *Pseudomonas aeruginosa* and their interactions with lipopolysaccharides. *Antimicrob Agents Chemother* 58:4420–4430. <https://doi.org/10.1128/AAC.02536-13>
  30. El Khoury M, Swain J, Sautrey G, Zimmermann L, Van Der Smissen P, Décout J-L, Mingeot-Leclercq M-P. 2017. Targeting bacterial cardiolipin enriched microdomains: an antimicrobial strategy used by amphiphilic aminoglycoside antibiotics. *Sci Rep* 7:10697. <https://doi.org/10.1038/s41598-017-10543-3>
  31. Sautrey G, El Khoury M, Dos Santos AG, Zimmermann L, Deleu M, Lins L, Décout J-L, Mingeot-Leclercq M-P. 2016. Negatively charged lipids as a potential target for new amphiphilic aminoglycoside antibiotics: a biophysical study. *J Biol Chem* 291:13864–13874. <https://doi.org/10.1074/jbc.M115.665364>
  32. Powers MJ, Trent MS. 2019. Intermembrane transport: glycerophospholipid homeostasis of the Gram-negative cell envelope. *Proc Natl Acad Sci U S A* 116:17147–17155. <https://doi.org/10.1073/pnas.1902026116>
  33. Shrivastava R, Jiang X, Chng S-S. 2017. Outer membrane lipid homeostasis via retrograde phospholipid transport in *Escherichia coli*: a physiological function for the Tol-Pal complex. *Mol Microbiol* 106:395–408.
  34. Giordano NP, Cian MB, Dalebroux ZD. 2020. Outer membrane lipid secretion and the innate immune response to Gram-negative bacteria. *Infect Immun* 88:1–21. <https://doi.org/10.1128/IAI.00920-19>
  35. Cian MB, Giordano NP, Mettlach JA, Minor KE, Dalebroux ZD. 2020. Separation of the cell envelope for Gram-negative bacteria into inner and outer membrane fractions with technical adjustments for *Acinetobacter baumannii*. *J Vis Exp* 60517. <https://doi.org/10.3791/60517>
  36. Palmer LD, Minor KE, Mettlach JA, Rivera ES, Boyd KL, Caprioli RM, Spraggins JM, Dalebroux ZD, Skaar EP. 2020. Modulating isoprenoid biosynthesis increases lipooligosaccharides and restores *Acinetobacter baumannii* resistance to host and antibiotic stress. *Cell Rep* 32:108129. <https://doi.org/10.1016/j.celrep.2020.108129>
  37. Lam JS, Taylor VL, Islam ST, Hao Y, Kocíncová D. 2011. Genetic and functional diversity of *Pseudomonas aeruginosa* lipopolysaccharide. *Front Microbiol* 2:118. <https://doi.org/10.3389/fmicb.2011.00118>
  38. Elhenawy W, Bording-Jorgensen M, Valguarnera E, Haurat MF, Wine E, Feldman MF. 2016. LPS remodeling triggers formation of outer membrane vesicles in *Salmonella*. *MBio* 7:1–12. <https://doi.org/10.1128/mBio.00940-16>
  39. Simpson BW, Trent MS. 2019. Pushing the envelope: LPS modifications and their consequences. *Nat Rev Microbiol* 17:403–416. <https://doi.org/10.1038/s41579-019-0201-x>
  40. King JD, Kocíncová D, Westman EL, Lam JS. 2009. Review: lipopolysaccharide biosynthesis in *Pseudomonas aeruginosa*. *Innate Immun* 15:261–312. <https://doi.org/10.1177/1753425909106436>
  41. Krieg M, Fläschner G, Alsteens D, Gaub BM, Roos WH, Wuite GJL, Gaub HE, Gerber C, Dufrène YF, Müller DJ. 2019. Atomic force microscopy-based mechanobiology. *Nat Rev Phys* 1:41–57. <https://doi.org/10.1038/s42254-018-0001-7>
  42. Mathélié-Guinlet M, Asmar AT, Collet JF, Dufrène YF. 2020. Lipoprotein lpp regulates the mechanical properties of the *E. coli* cell envelope. *Nat Commun* 11:1789. <https://doi.org/10.1038/s41467-020-15489-1>
  43. Arnoldi M, Fritz M, Bäuerlein E, Radmacher M, Sackmann E, Boulbitch A. 2000. Bacterial turgor pressure can be measured by atomic force microscopy. *Phys Rev E* 62:1034–1044. <https://doi.org/10.1103/PhysRevE.62.1034>

44. Touhami A, Nysten B, Dufréne YF. 2003. Nanoscale mapping of the elasticity of microbial cells by atomic force microscopy. *Langmuir* 19:4539–4543. <https://doi.org/10.1021/la034136x>
45. Formosa C, Grare M, Jauvert E, Coutable A, Regnouf-de-Vains JB, Mourer M, Duval RE, Dague E. 2012. Nanoscale analysis of the effects of antibiotics and CX1 on a *Pseudomonas aeruginosa* multidrug-resistant strain. *Sci Rep* 2:575. <https://doi.org/10.1038/srep00575>
46. Cerf A, Cau JC, Vieu C, Dague E. 2009. Nanomechanical properties of dead or alive single-patterned bacteria. *Langmuir* 25:5731–5736. <https://doi.org/10.1021/la9004642>
47. Longo G, Rio LM, Roduit C, Trampuz A, Bizzini A, Dietler G, Kasas S. 2012. Force volume and stiffness tomography investigation on the dynamics of stiff material under bacterial membranes. *J Mol Recognit* 25:278–284. <https://doi.org/10.1002/jmr.2171>
48. Mathelié-Guinlet M, Grauby-Heywang C, Martin A, Février H, Moroté F, Vilquin A, Béven L, Delville MH, Cohen-Bouhacina T. 2018. Detrimental impact of silica nanoparticles on the nanomechanical properties of *Escherichia coli*, studied by AFM. *J Colloid Interface Sci* 529:53–64. <https://doi.org/10.1016/j.jcis.2018.05.098>
49. Yao X, Jericho M, Pink D, Beveridge T. 1999. Thickness and elasticity of Gram-negative murein sacculi measured by atomic force microscopy. *J Bacteriol* 181:6865–6875. <https://doi.org/10.1128/JB.181.22.6865-6875.1999>
50. Mortensen NP, Fowlkes JD, Sullivan CJ, Allison DP, Larsen NB, Molin S, Doktycz MJ. 2009. Effects of colistin on surface ultrastructure and nanomechanics of *Pseudomonas aeruginosa* cells. *Langmuir* 25:3728–3733. <https://doi.org/10.1021/la803898g>
51. Vitiello G, Oliva R, Petraccone L, Vecchio PD, Heenan RK, Molinaro A, Silipo A, D'Errico G, Paduano L. 2021. Covalently bonded hopanoid-lipid A from *Bradyrhizobium*: the role of unusual molecular structure and calcium ions in regulating the lipid bilayers organization. *J Colloid Interface Sci* 594:891–901. <https://doi.org/10.1016/j.jcis.2021.03.072>
52. Korneev KV, Arbatsky NP, Molinaro A, Palmigiano A, Shaikhutdinova RZ, Shneider MM, Pier GB, Kondakova AN, Sviriaeva EN, Sturiale L, Garozzo D, Kruglov AA, Nedospasov SA, Drutskaya MS, Knirel YA, Kuprash DV. 2015. Structural relationship of the lipid A acyl groups to activation of murine toll-like receptor 4 by lipopolysaccharides from pathogenic strains of *Burkholderia mallei*, *Acinetobacter baumannii*, and *Pseudomonas aeruginosa*. *Front Immunol* 6:595. <https://doi.org/10.3389/fimmu.2015.00595>
53. Gaboriaud F, Baillet S, Dague E, Jorand F. 2005. Surface structure and nanomechanical properties of *Shewanella putrefaciens* bacteria at two pH values (4 and 10) determined by atomic force microscopy. *J Bacteriol* 187:3864–3868. <https://doi.org/10.1128/JB.187.11.3864-3868.2005>
54. Beckmann MA, Venkataraman S, Doktycz MJ, Nataro JP, Sullivan CJ, Morrell-Falvey JL, Allison DP. 2006. Measuring cell surface elasticity on enteroaggregative *Escherichia coli* wild type and dispersin mutant by AFM. *Ultramicroscopy* 106:695–702. <https://doi.org/10.1016/j.ultramicro.2006.02.006>
55. Velegol SB, Logan BE. 2002. Contributions of bacterial surface polymers, electrostatics, and cell elasticity to the shape of AFM force curves. *Langmuir* 18:5256–5262. <https://doi.org/10.1021/la011818g>
56. Mozaheb N, Van Der Smissen P, Opsomer T, Mignolet E, Terrasi R, Paquot A, Larondelle Y, Dehaen W, Muccioli GG, Mingeot-Leclercq M-P. 2022. Contribution of membrane vesicle to reprogramming of bacterial membrane fluidity in *Pseudomonas aeruginosa*. *mSphere* 7:e0018722. <https://doi.org/10.1128/msphere.00187-22>
57. Kuimova MK, Yahioglu G, Levitt JA, Suhring K. 2008. Molecular rotor measures viscosity of live cells via fluorescence lifetime imaging. *J Am Chem Soc* 130:6672–6673. <https://doi.org/10.1021/ja800570d>
58. Vaara M, Plachy WZ, Nikaido H. 1990. Partitioning of hydrophobic probes into lipopolysaccharide bilayers. *Biochim et Biophys Acta (BBA) - Biomembranes* 1024:152–158. [https://doi.org/10.1016/0005-2736\(90\)90218-D](https://doi.org/10.1016/0005-2736(90)90218-D)
59. Hancock RE, Wong PG. 1984. Compounds which increase the permeability of the *Pseudomonas aeruginosa* outer membrane. *Antimicrob Agents Chemother* 26:48–52. <https://doi.org/10.1128/AAC.26.1.48>
60. Sutterlin HA, Shi H, May KL, Miguel A, Khare S, Huang KC, Silhavy TJ. 2016. Disruption of lipid homeostasis in the Gram-negative cell envelope activates a novel cell death pathway. *Proc Natl Acad Sci U S A* 113:E1565–E1574. <https://doi.org/10.1073/pnas.1601375113>
61. Nakamura S, Shchepetov M, Dalia AB, Clark SE, Murphy TF, Sethi S, Gilsdorf JR, Smith AL, Weiser JN. 2011. Molecular basis of increased serum resistance among pulmonary isolates of non-typeable *Haemophilus influenzae*. *PLoS Pathog* 7:e1001247. <https://doi.org/10.1371/journal.ppat.1001247>
62. Kamischke C, Fan J, Bergeron J, Kulasekara HD, Dalebroux ZD, Burrell A, Kollman JM, Miller SI. 2019. The *Acinetobacter baumannii* Mla system and glycerophospholipid transport to the outer membrane. *Elife* 8:1–25. <https://doi.org/10.7554/eLife.40171>
63. Shen L, Gao X, Wei J, Chen L, Zhao X, Li B, Duan K. 2012. PA2800 plays an important role in both antibiotic susceptibility and virulence in *Pseudomonas aeruginosa*. *Curr Microbiol* 65:601–609. <https://doi.org/10.1007/s00284-012-0196-2>
64. Guest RL, Rutherford ST, Silhavy TJ. 2021. Border control: regulating LPS biogenesis. *Trends Microbiol* 29:334–345. <https://doi.org/10.1016/j.tim.2020.09.008>
65. Ouberaï M, El Garch F, Bussiere A, Riou M, Alsteens D, Lins L, Baussanne I, Dufréne YF, Brasseur R, Decout JL, Mingeot-Leclercq MP. 2011. The *Pseudomonas aeruginosa* membranes: a target for a new amphiphilic aminoglycoside derivative? *Biochim et Biophys Acta (BBA) - Biomembranes* 1808:1716–1727. <https://doi.org/10.1016/j.bbame.2011.01.014>
66. Fivenson EM, Bernhardt TG. 2020. An essential membrane protein modulates the proteolysis of LpxC to control lipopolysaccharide synthesis in *Escherichia coli*. *MBio* 11:1–12. <https://doi.org/10.1128/mBio.00939-20>
67. Nguyen M, Gautier T, Reocreux G, Pallot G, Maquart G, Bahr P-A, Tavernier A, Grober J, Masson D, Bouhemad B, Guinot P-G. 2021. Increased phospholipid transfer protein activity is associated with markers of enhanced lipopolysaccharide clearance in human during cardiopulmonary bypass. *Front Cardiovasc Med* 8:756269. <https://doi.org/10.3389/fcvm.2021.756269>
68. Wahl A, My L, Dumoulin R, Sturgis JN, Bouveret E. 2011. Antagonistic regulation of *dgkA* and *plsB* genes of phospholipid synthesis by multiple stress responses in *Escherichia coli*. *Mol Microbiol* 80:1260–1275. <https://doi.org/10.1111/j.1365-2958.2011.07641.x>
69. Emiola A, Andrews SS, Heller C, George J. 2016. Crosstalk between the lipopolysaccharide and phospholipid pathways during outer membrane biogenesis in *Escherichia coli*. *Proc Natl Acad Sci U S A* 113:3108–3113. <https://doi.org/10.1073/pnas.1521168113>
70. Thomanek N, Arends J, Lindemann C, Barkovits K, Meyer HE, Marcus K, Narberhaus F. 2018. Intricate crosstalk between lipopolysaccharide, phospholipid and fatty acid metabolism in *Escherichia coli* modulates proteolysis of LpxC. *Front Microbiol* 9:3285. <https://doi.org/10.3389/fmicb.2018.03285>
71. Anderson MS, Raetz CR. 1987. Biosynthesis of lipid A precursors in *Escherichia coli*. A cytoplasmic acyltransferase that converts UDP-N-acetylglucosamine to UDP-3-O-(R-3-hydroxymyristoyl)-N-acetylglucosamine. *J Biol Chem* 262:5159–5169. [https://doi.org/10.1016/S0021-9258\(18\)61169-X](https://doi.org/10.1016/S0021-9258(18)61169-X)
72. Douglass MV, Cléon F, Trent MS. 2021. Cardiolipin AIDs in lipopolysaccharide transport to the gram-negative outer membrane. *Proc Natl Acad Sci U S A* 118:e2018329118. <https://doi.org/10.1073/pnas.2018329118>
73. Powers MJ, Simpson BW, Trent MS. 2020. The Mla pathway in *Acinetobacter baumannii* has no demonstrable role in anterograde lipid transport. *Elife* 9:1–21. <https://doi.org/10.7554/eLife.56571>
74. Son M, London E. 2013. The dependence of lipid asymmetry upon polar headgroup structure. *J Lipid Res* 54:3385–3393. <https://doi.org/10.1194/jlr.M041749>
75. de Jonge EF, van Boxel R, Balhuizen MD, Haagsman HP, Tommassen J. 2022. Pal depletion results in hypervisculation and affects cell morphology and outer-membrane lipid asymmetry in bordetellae. *Res Microbiol* 173:103937. <https://doi.org/10.1016/j.resmic.2022.103937>
76. Paulsson M, Kragh KN, Su YC, Sandblad L, Singh B, Bjarnsholt T, Riesbeck K. 2021. Peptidoglycan-binding anchor is a *Pseudomonas aeruginosa* OmpA family lipoprotein with importance for outer membrane vesicles, biofilms, and the periplasmic shape. *Front Microbiol* 12:639582. <https://doi.org/10.3389/fmicb.2021.639582>

77. Baarda BI, Zielke RA, Le Van A, Jerse AE, Sikora AE. 2019. *Neisseria gonorrhoeae* MlaA influences gonococcal virulence and membrane vesicle production. *PLoS Pathog* 15:e1007385. <https://doi.org/10.1371/journal.ppat.1007385>
78. Batista JH, Leal FC, Fukuda TTH, Alcoforado Diniz J, Almeida F, Pupo MT, da Silva Neto JF. 2020. Interplay between two quorum sensing-regulated pathways, violacein biosynthesis and VacJ/Yrb, dictates outer membrane vesicle biogenesis in *Chromobacterium violaceum*. *Environ Microbiol* 22:2432–2442. <https://doi.org/10.1111/1462-2920.15033>
79. Davies C, Taylor AJ, Elmi A, Winter J, Liaw J, Grabowska AD, Gundogdu O, Wren BW, Kelly DJ, Dorrell N. 2019. Sodium taurocholate stimulates *Campylobacter jejuni* outer membrane vesicle production via down-regulation of the maintenance of lipid asymmetry pathway. *Front Cell Infect Microbiol* 9:177. <https://doi.org/10.3389/fcimb.2019.00177>
80. Roier S, Zingl FG, Cakar F, Durakovic S, Kohl P, Eichmann TO, Klug L, Gadermaier B, Weinzerl K, Prassl R, Lass A, Daum G, Reidl J, Feldman MF, Schild S. 2016. A novel mechanism for the biogenesis of outer membrane vesicles in Gram-negative bacteria. *Nat Commun* 7:10515. <https://doi.org/10.1038/ncomms10515>
81. Nasu H, Shirakawa R, Furuta K, Kaito C. 2022. Knockout of *mIaA* increases *Escherichia coli* virulence in a silkworm infection model. *PLoS One* 17:e0270166. <https://doi.org/10.1371/journal.pone.0270166>
82. Cooke IR, Deserno M. 2006. Coupling between lipid shape and membrane curvature. *Biophys J* 91:487–495. <https://doi.org/10.1529/biophysj.105.078683>
83. Dowhan W. 1997. Molecular basis for membrane phospholipid diversity: why are there so many lipids? *Annu Rev Biochem* 66:199–232. <https://doi.org/10.1146/annurev.biochem.66.1.199>
84. Graham TR, Kozlov MM. 2010. Interplay of proteins and lipids in generating membrane curvature. *Curr Opin Cell Biol* 22:430–436. <https://doi.org/10.1016/j.cob.2010.05.002>
85. Werneburg M, Zerbe K, Juhas M, Bigler L, Stalder U, Kaech A, Ziegler U, Obrecht D, Eberl L, Robinson JA. 2012. Inhibition of lipopolysaccharide transport to the outer membrane in *Pseudomonas aeruginosa* by peptidomimetic antibiotics. *Chembiochem* 13:1767–1775. <https://doi.org/10.1002/cbic.201200276>
86. Chowdhury C, Jagannadham MV. 2013. Virulence factors are released in association with outer membrane vesicles of *Pseudomonas syringae* pv. tomato T1 during normal growth. *Biochim et Biophys Acta (BBA) - Proteins Proteomics* 1834:231–239. <https://doi.org/10.1016/j.bbapap.2012.09.015>
87. Kulkarni HM, Jagannadham MV. 2014. Biogenesis and multifaceted roles of outer membrane vesicles from Gram-negative bacteria. *Microbiology (Reading, Engl)* 160:2109–2121. <https://doi.org/10.1099/mic.0.079400-0>
88. Schlame M, Rua D, Greenberg ML. 2000. The biosynthesis and functional role of cardiolipin. *Prog Lipid Res* 39:257–288. [https://doi.org/10.1016/s0163-7827\(00\)00005-9](https://doi.org/10.1016/s0163-7827(00)00005-9)
89. Kudryakova IV, Suzina NE, Vinokurova NG, Shishkova NA, Vasilyeva NV. 2017. Studying factors involved in biogenesis of *Lyso bacter* sp. XL1 outer membrane vesicles. *Biochemistry Moscow* 82:501–509. <https://doi.org/10.1134/S0006297917040125>
90. Bonnington KE, Kuehn MJ. 2016. Outer membrane vesicle production facilitates LPS remodeling and outer membrane maintenance in *Salmonella* during environmental transitions. *MBio* 7:e01532-16. <https://doi.org/10.1128/mBio.01532-16>
91. Florez C, Raab JE, Cooke AC, Schertzer JW. 2017. Membrane distribution of the *Pseudomonas* quinolone signal modulates outer membrane vesicle production in *Pseudomonas aeruginosa*. *MBio* 8:1–13. <https://doi.org/10.1128/mBio.01034-17>
92. Mashburn LM, Whiteley M. 2005. Membrane vesicles traffic signals and facilitate group activities in a prokaryote. *Nature New Biol* 437:422–425. <https://doi.org/10.1038/nature03925>
93. Schwachheimer C, Kulp A, Kuehn MJ. 2014. Modulation of bacterial outer membrane vesicle production by envelope structure and content. *BMC Microbiol* 14:324. <https://doi.org/10.1186/s12866-014-0324-1>
94. Kawasaki K, Manabe T. 2010. Latency of the lipid A deacylase PagL is involved in producing a robust permeation barrier in the outer membrane of *Salmonella enterica*. *J Bacteriol* 192:5837–5840. <https://doi.org/10.1128/JB.00758-10>
95. Gunn JS, Belden WJ, Miller SI. 1998. Identification of PhoP-PhoQ activated genes within a duplicated region of the *Salmonella typhimurium* chromosome. *Microb Pathog* 25:77–90. <https://doi.org/10.1006/mpat.1998.0217>
96. Klein S, Lorenzo C, Hoffmann S, Walther JM, Storbeck S, Piekarski T, Tindall BJ, Wray V, Nimtz M, Moser J. 2009. Adaptation of *Pseudomonas aeruginosa* to various conditions includes tRNA-dependent formation of alanyl-phosphatidylglycerol. *Mol Microbiol* 71:551–565. <https://doi.org/10.1111/j.1365-2958.2008.06562.x>
97. Sabnis A, Hagart KL, Klöckner A, Becce M, Evans LE, Furniss RCD, Mavridou DA, Murphy R, Stevens MM, Davies JC, Larrouy-Maumus GJ, Clarke TB, Edwards AM. 2021. Colistin kills bacteria by targeting lipopolysaccharide in the cytoplasmic membrane. *Elife* 10:e65836. <https://doi.org/10.7554/eLife.65836>
98. Diaz Iglesias Y, Van Bambeke F. 2020. Activity of antibiotics against *Pseudomonas aeruginosa* in an *in vitro* model of biofilms in the context of cystic fibrosis: influence of the culture medium. *Antimicrob Agents Chemother* 64:e02204-19. <https://doi.org/10.1128/AAC.02204-19>
99. Pompilio A, Crocetta V, Pomponio S, Fiscarelli E, Di Bonaventura G. 2015. *In vitro* activity of colistin against biofilm by *Pseudomonas aeruginosa* is significantly improved under “cystic fibrosis-like” physicochemical conditions. *Diagn Microbiol Infect Dis* 82:318–325. <https://doi.org/10.1016/j.diagmicrobio.2015.01.006>
100. Quinn RA, Comstock W, Zhang T, Morton JT, da Silva R, Tran A, Aksenov A, Nothias L-F, Wangpraseurt D, Melnik AV, Ackermann G, Conrad D, Klapper I, Knight R, Dorrestein PC. 2018. Niche partitioning of a pathogenic microbiome driven by chemical gradients. *Sci Adv* 4:eaau1908. <https://doi.org/10.1126/sciadv.aau1908>
101. Baussanne I, Bussière A, Halder S, Ganem-Elbaz C, Ouberai M, Riou M, Paris JM, Ennifar E, Mingeot-Leclercq MP, Décourt JL. 2010. Synthesis and antimicrobial evaluation of amphiphilic neamine derivatives. *J Med Chem* 53:119–127. <https://doi.org/10.1021/jm900615h>
102. Hmelo LR, Borlee BR, Almblad H, Love ME, Randall TE, Tseng BS, Lin C, Irie Y, Storek KM, Yang JJ, Siehnell RJ, Howell PL, Singh PK, Tolker-Nielsen T, Parsek MR, Schweizer HP, Harrison JJ. 2015. Precision-engineering the *Pseudomonas aeruginosa* genome with two-step allelic exchange. *Nat Protoc* 10:1820–1841. <https://doi.org/10.1038/nprot.2015.115>
103. Rietsch A, Vallet-Gely I, Dove SL, Mekalanos JJ. 2005. ExsE, a secreted regulator of type III secretion genes in *Pseudomonas aeruginosa*. *Proc Natl Acad Sci U S A* 102:8006–8011. <https://doi.org/10.1073/pnas.0503005102>
104. Ude J, Tripathi V, Buyck JM, Söderholm S, Cunrath O, Fanous J, Claudi B, Egli A, Schleberger C, Hiller S, Bumann D. 2021. Outer membrane permeability: antimicrobials and diverse nutrients bypass porins in *Pseudomonas aeruginosa*. *Proc Natl Acad Sci U S A* 118:e2107644118. <https://doi.org/10.1073/pnas.2107644118>
105. Choi K-H, Schweizer HP. 2006. Mini-Tn7 insertion in bacteria with single attTn7 sites: example *Pseudomonas aeruginosa*. *Nat Protoc* 1:153–161. <https://doi.org/10.1038/nprot.2006.24>
106. Lee CH, Tsai CM. 1999. Quantification of bacterial lipopolysaccharides by the purpald assay: measuring formaldehyde generated from 2-keto-3-deoxyoctonate and heptose at the inner core by periodate oxidation. *Anal Biochem* 267:161–168. <https://doi.org/10.1006/abio.1998.2961>
107. Quesenberry MS, Lee YC. 1996. A rapid formaldehyde assay using purpald reagent: application under periodation conditions. *Anal Biochem* 234:50–55. <https://doi.org/10.1006/abio.1996.0048>
108. Park HG, Sathiyarayanan G, Hwang CH, Ann DH, Kim JH, Bang G, Jang KS, Ryu HW, Lee YK, Yang YH, Kim YG. 2017. Chemical structure of the lipid A component of *Pseudomonas* sp. strain PAMC 28618 from thawing permafrost in relation to pathogenicity. *Sci Rep* 7:2168. <https://doi.org/10.1038/s41598-017-02145-w>
109. Sasser M. 2006. Technical note # 101 Microbial identification by gas chromatographic analysis of fatty acid methyl esters (GC-FAME). T N:1–6.
110. Cooke AC, Nello AV, Ernst RK, Schertzer JW. 2019. Analysis of *Pseudomonas aeruginosa* biofilm membrane vesicles supports multiple mechanisms of biogenesis. *PLoS ONE* 14:e0212275. <https://doi.org/10.1371/journal.pone.0212275>
111. Mizuno T, Kageyama M. 1979. Isolation and characterization of a major outer membrane protein of *Pseudomonas aeruginosa*: evidence for the occurrence of a lipoprotein. *J Biochem* 85:115–122. <https://doi.org/10.1093/oxfordjournals.jbchem.a132300>



112. Sader JE, Larson I, Mulvaney P, White LR. 1995. Method for the calibration of atomic force microscope cantilevers. *Rev Sci Instrum* 66:3789–3798. <https://doi.org/10.1063/1.1145439>
113. Thomas G, Burnham NA, Camesano TA, Wen Q. 2013. Measuring the mechanical properties of living cells using atomic force microscopy. *J Vis Exp*:50497. <https://doi.org/10.3791/50497>
114. Mika JT, Thompson AJ, Dent MR, Brooks NJ, Michiels J, Hofkens J, Kuimova MK. 2016. Measuring the viscosity of the *Escherichia coli* plasma membrane using molecular rotors. *Biophys J* 111:1528–1540. <https://doi.org/10.1016/j.bpj.2016.08.020>
115. Angus BL, Carey AM, Caron DA, Kropinski AM, Hancock RE. 1982. Outer membrane permeability in *Pseudomonas aeruginosa*: comparison of a wild-type with an antibiotic-supersusceptible mutant. *Antimicrob Agents Chemother* 21:299–309. <https://doi.org/10.1128/AAC.21.2.299>